



Role of the dew water on the ground surface in HONO distribution: a case measurement in Melpitz

Yangang Ren¹, Bastian Stieger², Gerald Spindler², Benoit Grosselin¹, Abdelwahid

5 Mellouki^{1*}, Thomas Tuch², Alfred Wiedensohler², Hartmut Herrmann^{2*},

1. Institut de Combustion, Aérothermique, Réactivité et Environnement (ICARE), CNRS
(UPR 3021), Observatoire des Sciences de l'Univers en région Centre (OSUC), 1C Avenue de
la Recherche Scientifique, 45071 Orléans Cedex 2, France

2. Leibniz Institute for Tropospheric Research (TROPOS), Permoserstraße 15, 04318 Leipzig,
10 Germany

* Corresponding author: Abdelwahid Mellouki (abdelwahid.mellouki@cnrs-orleans.fr) and
Hartmut Herrmann (herrmann@tropos.de)

Abstract: To characterize the role of dew water on the ground surface HONO distribution,
15 nitrous acid (HONO) measurements with a MARGA and a LOPAP instrument were
performed at the TROPOS research site in Melpitz from 19 to 29 April 2018. The dew water
was also collected and analyzed from 8 to 14 May 2019 using a glass sampler. The high-time
resolution of HONO measurements showed well-defined diurnal variations that revealed: (i)
20 vehicle emission is a minor source of HONO at the Melpitz station; (ii) heterogeneous
conversion of NO₂ to HONO on ground surface dominates HONO production at night; (iii)
significant nighttime ground surface deposition of HONO with a strength of sink of
0.161±0.122 ppbv h⁻¹; (iv) dew water with mean NO₂⁻ of 7.91±2.14 µg m⁻² could serve as a
temporary HONO source in the morning when the dew droplets evaporate. The nocturnal
25 observations of HONO and NO₂ allowed direct evaluation of the ground uptake coefficients
for these species at night: $\gamma_{\text{NO}_2 \rightarrow \text{HONO}} = 1.4 \times 10^{-6}$ to 1.5×10^{-5} , $\gamma_{\text{HONO,ground}} = 5.6$ to 19.5. A
chemical model demonstrated that HONO deposition to the ground surface at night was
90-100% of the calculated unknown HONO source in the morning. These results suggest that
30 dew water on the ground surface was controlling the temporal HONO distribution rather than
straightforward NO₂-HONO conversion. This can strongly enhance the OH reactivity
throughout morning time or other planted areas that provide large amount of ground surface
based on the OH production rate calculation.

Keywords: HONO, ground surface, NO₂-HONO conversion, dew water, OH production



35 1 Introduction

Nitrous acid (HONO) plays an important role in the atmospheric chemistry as its photolysis (reaction 1, all the reaction equations regarding on HONO sink and source were provided in Table S1) is proposed to be an important source of OH radicals. In the troposphere, OH radicals can initiate daytime photochemistry, leading to the formation of ozone (O₃) and secondary organic aerosol (SOA).

At present, the mechanisms of HONO formation have been and are still widely discussed. In the absence of light, heterogeneous reactions of NO₂ occur on wet surfaces (reaction 2) and is considered to be an important source of HONO according to both laboratory studies and field observations (Acker et al., 2004). Finlayson-Pitts et al. (2003) proposed a mechanism (reaction 2a) involving the formation of the NO₂ dimer (N₂O₄) especially during nighttime. However, this pathway is not important in the real atmosphere (Gustafsson et al., 2008). The surface of soot (Gutzwiller et al., 2002) or light induced soot (Monge et al., 2010) contain functionalities attached to the large carbonaceous structures or individual condensed organic species, like phenol (Gutzwiller et al., 2002) and light-activated humic acids (Stemmler et al., 2006), which undergo electron transfer reactions with NO₂ yielding HONO (reaction 2b). This reaction was also postulated for aromatics in the aqueous phase, but only proceeds at a relevant rate at high pH levels (Ammann et al., 2005; Lahoutifard et al., 2002). Gustafsson et al. (2008) provide the evidence that formation of HONO proceeds by a bimolecular reaction of absorbed NO₂ and H (reaction 2c) on mineral dust, where H formed from the dissociation of chemisorbed water. However, Finlayson-Pitts (2009) indicated that this pathway is probably not transferable from laboratory to real atmosphere. In addition to the direct emission from the vehicle exhaust (Kurtenbach et al., 2001) and homogeneous gas phase reaction of NO with OH (reaction 3) (Pagsberg et al., 1997) some other HONO formation mechanisms have been proposed, e.g. homogeneous reaction of NO, NO₂ and H₂O (reaction 4) (AndresHernandez et al., 1996) homogeneous nucleation of NO₂, H₂O, and NH₃ (reaction 5) (Zhang and Tao, 2010a) electronically excited NO₂ (NO₂^{*}) with water (reaction 6) (Finlayson-Pitts et al., 2003), high concentration of gaseous NO with HNO₃ on a “wet” surface (reaction 7) (Saliba et al., 2001) photolysis of nitric acid and nitrate (HNO₃/NO₃⁻) (reaction 8) (Ye et al., 2016; Zhou et al., 2011a) and nitrite emission from soil (reaction 9) (Su et al., 2011). However, the dominant HONO formation mechanism is still under discussion. Several studies (He et al., 2006; Rubio et al., 2009; Rubio et al., 2012; Acker et al., 2004; VandenBoer et al., 2013) reported that deposited HONO on wet surfaces can be a source for observed daytime HONO. Few of them have simultaneously quantified both dew and atmospheric composition. He et al. (2006) observed HONO released from a drying forest canopy and their lab studies show that, on average, ~90% of NO₂⁻ was emitted as HONO during dew evaporation. Rubio et al. (2009) found a positive correlation between



formaldehyde and HONO in dew and the atmosphere.

The dominant loss of HONO is photolysis during daytime, which forms OH radicals according to R1. An additional sink of HONO is the reaction with OH radical (reaction 10).

75 Due to the absence of solar radiation and the low OH concentration, the main loss process of HONO during nighttime is dry deposition, which can reach the balance with HONO production and vertical mixing to generate a steady state of HONO concentration. However, this is not the case in this work.

Due to its significant atmospheric importance, HONO has been measured for many years with various techniques (Platt et al., 1980; Kanda and Taira, 1990; Febo et al., 1993; Wang and Zhang, 2000; Schiller et al., 2001; Huang et al., 2002). LOPAP (long path absorption photometer) is a two channel in situ HONO measurement instrument, which detect HONO continuously by wet sampling and photometric detection. LOPAP is very selective without sampling artefact and chemical interferences (e.g. NO₂, NO, O₃, HCHO, HNO₃, SO₂ and PAN
85 etc.). In addition, the detection limit of LOPAP can go down to 3-6 pptv by optimizing the parameters like (a) sample gas flow rate, (b) liquid flow rates, and (c) the length of the absorption tubing (Heland et al., 2001). LOPAP was validated and compared with the most established and reliable HONO instrument DOAS (differential optical absorption spectroscopy), both in the field and a large simulation chamber under various conditions, and
90 found the excellent agreement (Heland et al., 2001; Kleffmann et al., 2006). MARGA (Monitor for Aerosols and Gases in ambient Air) is a commercial instrument combining a Steam-Jet Aerosol Collector (SJAC) and a Wet Rotating Denuder (WRD), which can quantify the inorganic water-soluble PM ions (Cl⁻, NO₃⁻, SO₄²⁻, NH₄⁺, Na⁺, K⁺, Mg²⁺, Ca²⁺) and corresponding trace gases (HCl, HONO, HNO₃, SO₂, NH₃). In recent years, MARGA
95 measurements were performed worldwide which has been summarized by Stieger et al. (2018), however, they determined a strong artefact of MARGA for HNO₃ measurement compared to a batch and coated denuder with shorter inlet. That induces an interesting objective of inter-comparison between MARGA and LOPAP for HONO measurement.

In this study, we present parallel measurements of HONO using LOPAP and MARGA in
100 Melpitz, Germany, over two weeks in 2018, and the dew water was also collected and analyzed from 8 to 14 May 2019 using two glass samplers. In addition, other water-soluble compounds, such as gaseous HNO₃, NH₃ and particulate NO₃⁻, SO₄²⁻, NH₄⁺, Na⁺, K⁺, Mg²⁺, Ca²⁺, trace gases (NO_x, SO₂ and O₃) and meteorological parameters were also measured simultaneously. Our observations provide the first inter-comparison between LOPAP and
105 MARGA for HONO field measurement, additional insights into HONO chemical formation processes and examine the relative importance of the HONO source.

2 Experimental



2.1 Site description

Measurements were performed at the research station of the Leibniz Institute for Tropospheric
110 Research (TROPOS) in Melpitz (12°56'E, 51°32'N). This rural field site is situated on a
meadow and surrounded by flat grass land, agricultural areas and forests. The Melpitz site
mainly can be influenced by two different wind direction: west wind origin from the marine
crossing a large area of Western Europe and the city of Leipzig (41 km NE), and east wind
crossing Eastern Europe (Spindler et al., 2004).

115 2.2 MARGA instrument

The MARGA (1S ADI 2080, The Netherlands) was used in this study and has already been
described in Stieger et al. (2018), so only short information was provided here. 1 m³ hr⁻¹ of air
was drawn into the sampling box after passing through an inside Teflon-coated PM₁₀ inlet
(URG, Chapel Hill, 3.5 m). Within the sample box, the sampled air laminarily passed a WRD
120 in which water-soluble gases diffuse into a 10 mg l⁻¹ hydrogen peroxide (H₂O₂) solution at
pH = 5.7. Particles can reach the SJAC because of their smaller diffusion velocities. Within
the SJAC, the particles grow into droplets under supersaturated water vapor conditions and
were collected by a cyclone. Then, the aqueous samples of the WRD (gas phase) and the
SJAC (particle phase) were successively injected into two ion-chromatographs (IC) with
125 conductivity detectors (Metrohm, Switzerland) by two syringe pumps (25 ml) for analyzing
the anions and cations. The Metrosep A Supp 10 (75/4.0) column and Metrosep C4 (100/4.0)
column were used to separate anions and cations, respectively. Lithium bromide was used as
the internal standard. The gas and particle samples are both collected in the course of one
hour.

130 2.3 LOPAP instrument

The LOPAP employed in this work was described in previous studies;(Bernard et al.,
2016;Heland et al., 2001) only brief description is given here. The LOPAP instrument consists
of two sections: a sampling unit and a detection unit. The sampling unit was composed of two
glass coils in series where the first coil (channel 1) accounted for HONO with interferences
135 and the second coil (channel 2) only interferences assuming that more than 99 % of HONO
was absorbed into acidic stripping solution (R1) to form diazonium salt in channel 1. This salt
reacts with solution R2 (0.8mM n-(1-naphthyl)ethylenediamine-dihydrochloride) to produce
final azo dye, which is photometrically detected by long path absorption in a special Teflon
tubing. Automatic air zero measurements were performed for 30 min per 12 h measurements
140 to correct for zero drifts. The temperature of the stripping coil was kept constant at 25 °C by a
thermostat.

To investigate the possible sampling inlet and denuder artefacts of the MARGA, two



different positions were settled for LOPAP during the measurement period (explained in SI):
M1, sampling unit of LOPAP was connected to the inlet of WRD in the back of the 2 m
145 sampling tube and the PM₁₀ inlet of MARGA as shown in Figure S1a (18 April 2018 13:00
UTC – 20 April 2018 08:00 UTC); M2 the sampling unit of LOPAP was settled in the same
level as the sampling head of MARGA (Figure S1b) (20th April 2018 15:00 UTC – 29 April
2018 07:00 UTC).

2.4 Dew water collecting and analysis

150 To evaluate the HONO emission from the dew water in the morning, the dew water was
collected and analyzed one year later on 8, 11, 13 and 14 May 2019. Similar conditions (grass
height, dew formation and day length) were observed to improve the evaluation. For dew
sampling, a glass sampler was used (as shown in Figure S2): two 1.5 m² glass plates were
placed 40 cm above the ground with a tilt angle of approximately 10°. A gutter was installed
155 at the lower end of each plates to collect the running down water. The water is trapped in 500
ml bottles. The dew samplers were prepared each evening before a likely dew event occurred
(low dew point difference, clear sky and low winds). Each plate was rinsed with at least 2 L
ultrapure water. A squeegee removed the excess water. Afterwards, the plates were cleaned
with ethanol and were again rinsed by 2 L ultrapure water. The plate was splashed with
160 ultrapure water and squeegeed six times and the gutter was cleaned. The sample of the sixth
splash was collected as blank.

The dew water normally was collected from 18:00 to 5:00 (UTC). In the morning, the
excess dew on the plate was squeegeed. To achieve the volume of dew (V_{dew}), the bottles were
weighted before and after sampling by a balance. The pH was measured by a pH meter (mod.
165 Lab 850, Schott Instruments). After sampling, the aqueous solutions were filtered and stored
in a fridge. Within six hours, the HONO analyses of the dew and blank samples were
performed by double-injection in the MARGA in the manual measurement mode as HONO
may volatilize between sampling and analysis. For the other ions (Cl⁻, NO₃⁻, SO₄²⁻, Oxalate,
Br⁻, F⁻, Formate, MSA, PO₄³⁻, Na⁺, NH₄⁺, K⁺ and Mg²⁺, Ca²⁺), the samples were analyzed
170 with laboratory ion chromatogram systems (mod. ICS-3000, Dionex, USA). Blanks from
water, the filter, the syringes and bottles were subtracted.

2.5 Aerosol measurements

The particle size distributions were measured in the size range from 5 nm to 10 μm
employing by a Dual Mobility Particle Size Spectrometer (TROPOS-type D-MPSS) (Birmili
175 et al., 1999) and an Aerodynamic Particle Size Spectrometer (APSS model 3321, TSI Inc.,
Shoreview, MN, USA). For the particle number size distribution measurements, the aerosol is
sampled through a low flow PM10 inlet and dried in an automatic diffusion dryer (Tuch et al.,



2009). The measurements and quality assurance are done following the recommendations given in Wiedensohler et al. (2012) and Wiedensohler et al. (2018). The MPSS derived
180 particle number size distribution was inverted by the algorithm described in Pfeifer et al. (2014), following the bipolar charge distribution of Wiedensohler (1988).

2.6 Other measurements

Trace gases of NO-NO₂-NO_x, SO₂ and O₃ were measured by NO_x analyzer (Thermo Model 42i-TL, Waltham, Massachusetts, USA), SO₂ analyzer APSA-360A and O₃ analyzer APOA
185 350 E (both Horiba, Kyoto, Japan) with a time resolutions of 1 min. It should be noted that NO₂ was converted to NO within the NO_x analyzer by a blue light converter BLC2 (Meteorologie Consult GmbH, Königstein, Germany). The provider for replacement of the Mo-Converter in the 42i-TL analyzer was MLU Messtechnik GmbH, Essen Germany. Meteorological parameters like temperature (T), precipitation, relative humidity (RH) as well
190 as wind velocity and direction were measured by PT1000, a rain gauge (R.M. Young Company, U.S.A.), the CS215 sensor (SensirionAG, Switzerland) and a WindSonic by Gill Instruments (UK), respectively. Global radiation and barometric pressure were recorded by a net radiometer CNR1 (Kipp&Zonen, The Netherlands) and a digital barometer (Vaisala, Germany), respectively.

195 2.7 Calculation of photolysis rate

Off-line NCAR Tropospheric Ultraviolet and Visible (TUV) transfer model (<https://www2.acom.ucar.edu/modeling/tropospheric-ultraviolet-and-visible-tuv-radiation-model>)
200 was used to estimate the photolysis rate of HONO (J_{HONO}), NO₂ (J_{NO_2}) and production rate of O¹D ($J_{\text{O}^1\text{D}}$) at the Melpitz station. Aerosol optical depth (AOD), total vertical ozone column, total NO₂ column, total cloud optical depth and surface reflectivity (Albedo) were taken from the NASA webpage for the period of measurement (<https://neo.sci.gsfc.nasa.gov/blog/>).

3 Results

3.1 Inter-comparison of LOPAP and MARGA

205 The hourly HONO mixing ratio obtained from MARGA was compared with the 30 seconds and hourly averaged HONO mixing ratios from LOPAP, respectively, as shown in Figure 1a and 1b. It indicates that the MARGA values were higher than the values of LOPAP but not during the peak events. The comparisons of the MARGA and LOPAP HONO measurements for period M1 and period M2 in Figure 1c result in slopes of 1.58 and 1.90 using Deming
210 regression, respectively.

Recently, Stieger et al. (2018) evaluated the HONO measurement of the on-line MARGA



system with another off-line batch denuder setup. The correlation was weak and the scatter large that is in agreement with the literature (Acker et al., 2004; Genfa et al., 2003). A possible reason was suggested by Genfa et al. (2003) in the use of different pH for the absorber solutions but this was not the case for the MARGA comparison with the batch denuder. More likely, is the different analysis time after sampling regarding on-line MARGA compared to off-line batch denuder. The evaporation of solved HONO from the off-line sample and heterogeneous reactions of NO₂ and H₂O as well as NO₂ and SO₂ in water described by Spindler et al. (2003) could explain the artefacts in the denuder solution (Kleffmann and Wiesen, 2008). Additional artefacts due to the long MARGA inlet system should be taken into account.

3.2 General results

Figure 2 and Figure 3 show an overview of the measured HONO, NO, NO₂, O₃, PM_{1.0}, PM_{2.5}, PM₁₀, meteorological parameters, water-soluble ions in PM₁₀ (NO₃⁻, SO₄²⁻, NH₄⁺, Na⁺, K⁺, Mg²⁺, Ca²⁺) and their corresponding trace gases (HONO, HNO₃, SO₂, NH₃) in the present study. The daytime (D, 04:00-18:00, UTC) and nighttime (N, 18:00-04:00) averages were also provided in Table 1. During the two weeks measurement, the prevailing winds were from the southwest and northwest sectors, indicating a possible influence of city emission from Leipzig, Germany, on the site. However, the strong wind (maximum 13 m s⁻¹) lead to a low PM concentration with low concentration of water-soluble ions in PM₁₀ (NO₃⁻, SO₄²⁻, NH₄⁺) and their corresponding trace gases (HNO₃, SO₂, NH₃) during the period 24-29 April 2018. The air temperature ranged from 5 °C to 27 °C and the RH showed a clear variation pattern with higher levels during the night and lower levels during daytime. During the campaign, good air quality was observed with daily averaged PM_{2.5} concentration of 15±4 µg m⁻³. In addition, low concentrations of NO and NO₂ with a diurnal average of 0.9±1.2 ppbv and 3.7±2.2 ppbv, respectively, were recorded. These observations highlight the nature of our measurement site as a typical background environment. The HONO concentration from the LOPAP measurements varied from 30 pptv to 1582 pptv and showed diurnal variations (with an average of 162±96 pptv and 254±114 pptv during daytime and nighttime, respectively) except for one case event, which will be discussed in the following section.

Größ et al. (2018) reported the linear function of the global radiation flux vs. OH radical concentration for the campaign EUCAARI 2008 at Melpitz.

$$[\text{OH}] = A \cdot \text{Rad} \quad (\text{Eq. 1})$$

with Rad being global solar irradiance in W m⁻² and [OH] is the hydroxyl radical concentration. The proportionality parameter A is 6110 m² W⁻¹ cm⁻³. On the basis of such a correlation, we derived the OH concentration during the period of this field measurement, with an average of (2.8±0.7)×10⁶ and (9.5±2.1)×10³ during daytime and nighttime,



respectively.

3.3 Diurnal variation of HONO, particles and trace gas species

250 The diurnal profiles of HONO and related supporting parameters are shown in Figure 4 for the whole period except for two case events: no HONO peak in the morning of 23 April and HONO peak observed at 0:00-2:00 (UTC) of 25 April (Figure 5). Overall, the HONO increased fast after the sunrise and peaked at 7:00 (UTC), which then dropped rapidly and reached a minimum at around 10:00 (UTC) and kept until 17:00 (UTC). This phenomenon
255 has been reported for Melpitz (4-14 April, 2008) by Acker et al. (2004), who expected that the storage of HONO on wet surfaces can be a source for observed daytime HONO. Such daytime pattern was also found in Spain, for a site surround by forests and sandy soils (Sörgel et al., 2011). Sörgel et al. (2011) explained this by local emissions which were trapped in the stable boundary layer before its breakup of the inversion in the morning based on a similar
260 diurnal cycle for NO and NO₂, which is different with this work. In this work, the NO₂ concentration decreased from the midnight until noon and NO peaked at 5:00 (UTC) then kept low concentrated (<1 ppbv) for 18 hours of one day. However, the diurnal variation trend of HONO during daytime was similar to that of HNO₃ and NH₃ in the gas phase as well as NO₃⁻ and NH₄⁺ in PM₁₀. This induced the explanation by the photolysis of adsorbed HNO₃
265 and NO₃⁻ (Zhou et al., 2011b; Zhou et al., 2003; Ye et al., 2016) and homogeneous nucleation of NO₂, H₂O and NH₃ (Zhang and Tao, 2010b). It was observed that dew was formed overnight during the campaign. Gaseous HONO could be deposited in these droplets. Due to evaporation after sunrise, HONO is reemitted in the atmosphere and lead to higher concentrations. This will be further discussed in Section 4.

270 As shown in Figure 4a and 4b, the HONO and NO₂ concentrations started to increase coincidentally at 16:00 (UTC) when the sunshine was weak. This was explained by the heterogeneous conversion of NO₂ to HONO during nighttime and will be discussed in Section 4. However, the HONO concentration then decreased from 21:00 (UTC) to around 100 pptv even though the NO₂ concentration kept constant around 5-6 ppbv. This decrease during
275 nighttime indicates the HONO loss process (dry and wet deposition, trapped in the boundary layer or dew etc.) surpassing the NO₂-to-HONO frequency. The diurnal cycle of O₃ reflects the balance between the photochemical formation of O₃ (e.g. NO₂ + hv) and O₃ consumption (e.g. ozonolysis of terpenes).

280 However, as illustrated in Figure 5, two case events were observed during the measurement period: (1) the HONO peak was not observed in the morning of 23rd April, 2018 without the parallel peak of gas-phase NO and NH₃ as well as NO₃⁻ and NH₄⁺ in PM₁₀; (2) due to the increase of wind speed, the HONO concentration climbed to 1.2 ppbv at around 0:00 (UTC) on 25 April 2018 and then decreased to 0.2 ppbv in one hour with the concurrent



increase of O₃.

285 3.4 HONO in the dew water

Dew water formation on canopy surfaces might be slightly acidic due to acid contribution from acidic aerosols (such as NH₄HSO₄) and could be an efficient removal pathway of water soluble pollutants. High solubility of HONO makes dew water an efficient sink and a stable reservoir for atmospheric HONO. Actually, a lot of dew water has been observed on the grass
290 around the Melpitz station during the sampling period of 19 to 29 April 2018. Hence, to investigate the dissolved HONO in the dew water of Melpitz station, the dew water was collected and analyzed from 8 to 14 May 2019 at the same season like the HONO measurements. Many ions e.g. NO₂⁻, Cl⁻, NO₃⁻, SO₄²⁻, Oxalate, Br⁻, F⁻, Formate, MSA, PO₄³⁻, Na⁺, NH₄⁺, K⁺ and Mg²⁺, Ca²⁺ were analyzed using MARGA and laboratory IC, but our
295 discussion only concern on NO₂⁻. The sample parameters (time, pH etc.) and NO₂⁻ concentration in the sample (μg L⁻¹) were shown in Table 2. The pH of dew water in Melpitz ranged from 6.30 to 7.00. It should be noted that the dew water was frozen until 1 hour after sunrise on 8, 13, 14 May 2019 but not on 11 May 2019. At this day, a third sample was collected sampled from 3:30 to 5:20 (UTC). The NO₂⁻ concentration per m² of the sampler
300 surface (F_{NO₂⁻}) was calculated from the following equation:

$$F_{\text{NO}_2^-} = \frac{[\text{NO}_2^-] \times V_{\text{dew}}}{1.5 \text{ m}^2 \times 1000} \quad (\text{Eq. 2})$$

Where [NO₂⁻] is the sample concentration in μg L⁻¹, V_{dew} is the sample volume in ml, 1.5 m² is the surface area of the glass sampler. As shown in Table 2, higher F_{NO₂⁻} was obtained on 11 May than on other days that were characterized by frozen dew water, which inhibited HONO
305 to dissolve. Then final F_{NO₂⁻} could be obtained by averaging F_{NO₂⁻} of the sum of the first and third sample with the second sample on 11 May resulting in 7.91±2.14 μg m⁻². This value will be used for the following calculation and discussion.

4 Discussion

4.1 Contribution of vehicle emissions

310 Since Melpitz site is close to a main national road from Leipzig to Torgau (Germany) that is within the main southwest wind direction, the contribution of vehicle emissions to the measured HONO concentrations should be evaluated. In generally, the HONO/NO_x ratio was usually chosen to derive the emission factor of HONO in the freshly emitted plumes (Kurtenbach et al., 2001) and the following five criteria were followed to select the cases:

- 315 (a) NO_x>45 ppbv;
(b) ΔNO/ΔNO_x>0.80;
(c) good correlation between HONO and NO_x (R² > 0.65);



(d) short duration of plumes (<2 h);

(e) global radiation < 10 W m⁻².

320 As illustrated in Figure S3, NO_x concentrations were lower than 15 ppbv and NO/NO_x ratio were lower than 0.8 (~0.4 in this campaign), suggesting the detected air is a mixture of fresh and aged air during the measurement period. Therefore, a substantial part of HONO is secondary. Additionally, the bad correlation between HONO and NO_x ($R^2 \approx 0.35$) suggests that the direct HONO emission from the vehicle emitted plumes were less important in this
325 work and, hence, be ignored in the following analysis.

4.2 Nighttime HONO

The nighttime HONO is different to some reported literatures (Li et al., 2012; Xianliang et al., 2007; Huang et al., 2017; Wang et al., 2017). HONO increased after sunset to a maximum at 21:00 (UTC) and decreased until sunrise. The OH concentration of $(9.5 \pm 2.1) \times 10^3$
330 molecule cm⁻³ (Table 1) together with NO mixing ratios during nighttime were used to estimate the net HONO production following Eq. 3 with $P_{OH+NO}^{net} = \sim 8.5 \times 10^{-5}$ ppbv h⁻¹. This extremely low value compared to other studies (Wong et al., 2011; Li et al., 2012) suggested that the contribution of gas-phase reaction of OH+NO to the nighttime HONO formation was negligible.

$$335 \quad P_{OH+NO}^{net} = k_{OH+NO}[OH][NO] - k_{OH+HONO}[OH][HONO] \quad (\text{Eq. 3})$$

4.2.1 Formation through heterogeneous conversion of NO₂

The ratio of [HONO]/[NO₂] was generally used as an index to estimate the efficiency of heterogeneous NO₂-HONO conversion because it is less influenced by transport processes than individual concentrations. However, the ratio might be influenced when a large fraction
340 of HONO is emitted from the traffic but this is expected to be less important as shown in section 4.1. Six cases as listed in Table 3 were selected to calculate the NO₂-HONO frequency following the criteria of Li et al. (2018):

(a) only the nighttime data in the absence of sunlight (i.e., 17:30-06:00 UTC) were used;

(b) both HONO concentrations and [HONO]/[NO₂] ratios increased steadily during the target
345 case;

(c) the meteorological conditions, especially surface winds, should be stable.

Figure S4 presents an example of the heterogeneous HONO formation occurring on 28 April 2018. In this case, the HONO mixing ratios increased rapidly after sunset from 100 pptv to 600 pptv. Together with the HONO concentrations, the [HONO]/[NO₂] ratio increased almost
350 linearly between 18:00 to 19:50 UTC. The slope fitted by the least linear regression for [HONO]/[NO₂] ratios against time can be taken as the conversion frequency of NO₂-to-HONO (k_{het}).



$$k_{\text{het}} = \frac{\frac{[\text{HONO}](t_2)}{[\text{NO}_2](t_2)} - \frac{[\text{HONO}](t_1)}{[\text{NO}_2](t_1)}}{t_2 - t_1} \quad (\text{Eq.4})$$

The covariation between [HONO] and [NO₂] during early nighttime (17:30-00:00 UTC) is shown in the correlations plot (Figure 6) that shows also the dependence of the [HONO]/[NO₂] ratios on the RH. As higher HONO concentration is usually found at higher RH level, the nighttime HONO formation is caused by reaction 2 (heterogeneous conversion of NO₂ to HONO). The ratio of [HONO]/[NO₂] during the Melpitz campaign ranged from 0.01 (1%) to <0.3 (30%) with mean value of 0.113±0.044. This mean values are within the wide range of reported values 0.008-0.13 in the fresh air masses from the most sampling sites (Alicke et al., 2002; Alicke et al., 2003; Xianliang et al., 2007; Su et al., 2008; Sörgel et al., 2011; Wang et al., 2017) except for the study of Yu et al. (2009), who got a high value as 0.3. However, to our best knowledge, this work presents also a high NO₂-to-HONO conversion frequency k_{het} of 0.027±0.017 h⁻¹ compared with most of the previous studies at urban sites, such as Wang et al. (2013) in Shanghai (0.007 h⁻¹), Alicke et al. (2002) in Milan (0.014 h⁻¹), Wang et al. (2017) in Beijing (0.008 h⁻¹) and Huang et al. (2017) in Xi'an (0.0091 h⁻¹). However, our value is comparable to Li et al. (2012) with 0.024±0.015 h⁻¹ and Alicke et al. (2003) with 0.018±0.009 h⁻¹, who also conducted rural measurements in the Pearl River Delta (PRD) area in Southern China and in Pabstthum, Germany, respectively, surrounded by farmland (grasses, trees, small forests).

4.2.2 Relative importance of particle and ground surface in nocturnal HONO production

The particle surface density S_a was calculated from the particle size distribution (Figure S5) ranged from 5 nm to 10 μm of APSS and D-MPSS data by assuming the particle are in spherical shape. The particle surface density S_a was further corrected with a hygroscopic factor $f(\text{RH})$ following the method of Li et al. (2012). Figure S6 illustrates the correlation between HONO, [HONO]/[NO₂] and S_a . Since the HONO concentration started to decrease from the midnight, the time range of 17:30-22:00 (UTC) was used to conduct the analysis. Both HONO and [HONO]/[NO₂] present a positive correlation with S_a , which indicate the HONO formation through the heterogeneous conversion of NO₂ on the particle surfaces. However, regarding to the weak correlation of [HONO]/[NO₂] with S_a ($R^2=0.208$), relative amount of HONO formed on particle surfaces might be small.

The formation of HONO through heterogeneous NO₂ conversion on particle surfaces (S_a) can be approximated following the recommendations in Li et al. (2010):

$$k_{\text{het}} = \frac{1}{4} \gamma_{\text{NO}_2 \rightarrow \text{HONO}_a} \times v_{\text{NO}_2} \times \frac{S_a}{V} \quad (\text{Eq.5})$$

where v_{NO_2} is the mean molecular velocity of NO₂ (370 m s⁻¹) (Ammann et al., 1998); S_a/V is the particle surface to volume ratio (m⁻¹) representing the surfaces available for heterogeneous



reaction, and $\gamma_{\text{NO}_2 \rightarrow \text{HONO}_a}$ is the uptake coefficient of NO_2 at the particle surface. If the entire HONO formation was taking place on the particle surface, the calculated $\gamma_{\text{NO}_2 \rightarrow \text{HONO}_a}$ varied
390 from 5.6×10^{-16} to 5.5×10^{-15} with a mean value of $2.1 \pm 1.2 \times 10^{-15}$. This extremely low value is in agreement with uptake coefficients of approximately 10^{-9} reported by Ndour et al. (2008), on all mineral solid surfaces without irradiation. Hence, this work concludes that, as previously reported (Wong et al., 2011; Sörgel et al., 2011; Kalberer et al., 1999), the HONO formation through heterogeneous NO_2 conversion on particle surfaces needs to be regarded as
395 non-significant.

As illustrated above, the heterogeneous NO_2 conversion on ground surfaces (including surfaces such as plants, building, soils etc.) contributes mainly to nighttime formation of HONO, which can be approximated by:

$$k_{\text{het}} = \frac{1}{8} \gamma_{\text{NO}_2 \rightarrow \text{HONO}_g} \times v_{\text{NO}_2} \times \frac{S_g}{V} \quad (\text{Eq.6})$$

400 where $\gamma_{\text{NO}_2 \rightarrow \text{HONO}_g}$ is the uptake coefficient of NO_2 at the ground surface, S_g/V represents the ground surface to volume ratio. As described by Zhang et al. (2016), the leaf area index (LAI, m^2/m^2) was used to estimate the surface to volume ratio for the vegetation-covered areas, following the method in Sarwar et al. (2008):

$$\frac{S_g}{V} = \frac{2 \times \text{LAI}}{H} \quad (\text{Eq.7})$$

405 Where H is the mixing layer height, taken from the study of Altstädter et al. (2018), who identified a heterogeneous lower atmospheric structure with the ceilometer data and observed a depth of less than 600 m from midnight until around 07:00 UTC in April 2014. LAI is multiplied by a factor of 2 to take the areas on both sides of the leaves into account. LAI is around 4 to 10 for grassland values. In Wohlfahrt et al. (2001), the LAI for meadows with
410 different heights are given. Regarding the height (~ 30 cm) in April 2018, we add a factor of 6. If the entire HONO formation was taking place on the ground surface, the calculated $\gamma_{\text{NO}_2 \rightarrow \text{HONO}_g}$ varied from 1.4×10^{-6} to 1.5×10^{-5} with a mean value of $7.1 \pm 4.4 \times 10^{-6}$. This value agrees well with the reported range of $\gamma_{\text{NO}_2 \rightarrow \text{HONO}}$ from 10^{-6} to 10^{-5} on the ground surface based on the laboratory studies (Kurtenbach et al., 2001; Kleffmann et al., 1998) and field
415 campaign in Colorado, USA (VandenBoer et al., 2013). It should be noted that the obtained NO_2 uptake coefficient on the ground surface is larger than the reactive surface provided by aerosols, suggesting that the heterogeneous reactions of NO_2 on ground surface may play a dominant role for the nighttime HONO formation.

4.2.3 HONO deposition on the ground surface

420 As illustrated in Figure 4a and S4, between midnight and sunrise (22:00-4:00 UTC), the deposition of HONO becomes increasingly important as the absolute amount of HONO decreased. Assuming a constant conversion frequency of NO_2 -to-HONO, k_{het} , the HONO



deposition rate (L_{HONO}) can be roughly estimated by:

$$L_{\text{HONO}} = \frac{d[\text{HONO}]}{dt} - k_{\text{het}} \times [\text{NO}_2] \quad (\text{Eq. 8})$$

425 The strength of the HONO sink during night is average 0.161 ± 0.122 ppbv h^{-1} and ranged from 0.041 to 0.447 ppbv h^{-1} . This value is higher than reported in the literature (Li et al., 2012) in the range of 0.06-0.11 ppbv h^{-1} . By integrating L_{HONO} from 22:00 to 4:00 (UTC), an accumulated HONO deposition on the ground surface of 966 ± 732 pptv can be derived.

The relationship of $[\text{HONO}]/[\text{NO}_2]$ with RH during nighttime (18:00-04:00) is illustrated
430 in Figure 7a. A positive trend of $[\text{HONO}]/[\text{NO}_2]$ ratio along the RH was found when RH was less than 70%, which is consistent with the kinetic of reaction (2). However, $[\text{HONO}]/[\text{NO}_2]$ performs a negative trend with RH for values over 70%. The same phenomenon was also observed by Yu et al. (2009) in Kathmandu and Li et al. (2012) in PRD region, China. This finding can be associated with larger amounts of dew water on various ground surfaces
435 (plants and grasses) when ambient humidity approached saturation, leading to an efficient uptake of HONO. The relationship of $[\text{HONO}]/[\text{NO}_2]$ with wind speed during nighttime (18:00-04:00) is illustrated in Figure 7b. As indicated in Figure 7b, wind speed was predominantly less than 3 m s^{-1} during the field campaign period in Melpitz and high conversion frequency of NO_2 -to-HONO mostly happened when wind speed was less than 1 m s^{-1} . However, some points show high $[\text{HONO}]/[\text{NO}_2]$ ratio happened when wind speed was in the range of 3 m s^{-1} to 4 m s^{-1} , mainly due to the evaporation of dew droplets resulting in the temporary HONO peak. Additionally, these samples indicate that the wind speed would also influence HONO deposition on the ground surface through decreasing RH (discussion in the following Section 4.3).

445 Assuming all the extra HONO were removed through deposition on the ground surface, the change of HONO in the time interval of 22:00-04:00 (UTC) was parameterized using a combination of Eq. 8 and the following equation:

$$L_{\text{HONO}} = \frac{1}{4} \gamma_{\text{HONO,ground}} \times [\text{HONO}] \times \frac{v_{\text{HONO,ground}}}{H} \quad (\text{Eq. 9})$$

Where $\gamma_{\text{HONO,ground}}$ is the HONO uptake coefficient on the ground surface, $v_{\text{HONO,ground}}$ is
450 the HONO deposition velocity and is 3.35 cm s^{-1} taken from the work of Spindler et al. (1999) at Melpitz within the nighttime H of 600 m. This approach yielded to a $\gamma_{\text{HONO,ground}}$ uptake coefficient in the range of 5.6 to 19.5, which is several orders higher than data found in Boulder, Colorado, ranging from 2×10^{-5} to 2×10^{-4} (VandenBoer et al., 2013). As observed by several studies (He et al., 2006; Rubio et al., 2009; Wentworth et al., 2016), the effective
455 Henry's law solubility of HONO is highly pH-dependent (from borderline soluble at $\text{pH} = 3$ to highly soluble at $\text{pH} \geq 6$), as would be expected for a weak acid. The Melpitz station is surrounded by grass land and tilled earth, the pH of collected dew water during nighttime in May 2019 was 6.3-7.0 (Table 2), where the effective Henry's law solubility of HONO would



be high. Furthermore, the amount of HONO in this dew water was quantified using MARGA
460 and ranged between 41.87 and 164.62 mg L⁻¹, which is higher than NO₂⁻ in Santiago's dew
waters (Rubio et al., 2009).

4.3 Daytime HONO

HONO concentrations started to increase after sunrise and peaked at 7:00 (UTC) (Figure 4),
during that time it also underwent photolysis, eventually reaching a steady state between
465 10:30–16:30 (UTC). Throughout the day, HONO was observed above an averaged minimum
mixing ratio of 98±15 pptv (10:30-16:30 UTC) with the maximum mixing ratio of 1400±100
pptv. Since NO and NO₂ have not the same diurnal cycle as HONO (Figure 4), the reactions
(2) and (3) are not expected to be responsible for this HONO morning peak, but could be the
main HONO source for period of 10:30-16:30 (UTC). It should be noted that gaseous NH₃,
470 HNO₃ and particulate NH₄⁺, NO₃⁻ also present the same trend like HONO as shown in Figure
4. Hence, two hypotheses would be proposed to explain the observed diurnal variations. The
first is that dew droplets on ground surfaces serve as a sink of HONO during the night and
become a morning source by releasing the trapped HONO back into ambient air, and the
second are photochemical processes such as reactions (6) and (8).

475 4.3.1 Photostationary state in the gas phase

The measured diurnal daytime HONO could be compared to model results by assuming an
instantaneous photo-equilibrium between the gas-phase formation (reaction 3 in Table S1) and
gas-phase loss processes (reactions 1 and 10 in Table S1), which is described by the following
expression (Kleffmann et al., 2005):

$$480 \quad [\text{HONO}]_{\text{pss}} = \frac{k_3[\text{OH}][\text{NO}]}{J_{\text{HONO}} + k_{10}[\text{OH}]} \quad (\text{Eq. 10})$$

OH concentration was estimated from linear function of the global radiation flux vs. OH
radical concentration as described in the previous section and shown in Figure 8b, J_{HONO} was
calculated using TUV model as described in section 2.6. The rate constants of NO+OH (k_3)
and HONO+OH (k_{10}) are referred to 7.4×10^{-12} cm³ molecule⁻¹ s⁻¹ (Burkholder et al., 2015) and
485 6.0×10^{-12} cm³ molecule⁻¹ s⁻¹ (Atkinson et al., 2004), respectively. As a result, shown in Figure
8b, the $[\text{HONO}]_{\text{pss}}$ (violet curve) could not explain the sudden HONO increase after sunrise
but indicates a HONO peak around 4:40 (UTC) according to the relatively high NO
concentration. However, some studies (Michoud et al., 2012; Sörgel et al., 2011) already
discussed that the stationary state of HONO can be only reached during noontime. Hence, a
490 model calculation (named Model1) was also used to discuss the HONO contribution from the
gas-phase reaction of NO with OH radical.

$$\frac{d[\text{HONO}]}{dt} = k_3[\text{OH}][\text{NO}] + k_{\text{het}} \times [\text{NO}_2] - J_{\text{HONO}}[\text{HONO}] - k_{10}[\text{HONO}][\text{OH}] \quad (\text{Eq. 11})$$



k_{het} derived from this work is 0.027 h^{-1} , $[\text{NO}]$ and $[\text{NO}_2]$ are averaged concentrations from this field measurement as shown in Figure 8a. The results are shown in Figure 8b
495 (orange line). It is reasonable to indicate that the reaction (3) only contribute 30-55% to the HONO increase in the early morning (4:30-7:30 UTC) Reaction (3) can continually contribute 50% (around $43 \pm 13 \text{ pptv}$) to the measured HONO ($98 \pm 15 \text{ pptv}$) from 10:30 to 16:30 (UTC). The additional HONO contribution rate could be estimated from following equation:

$$P_{\text{unknown}} = \frac{d[\text{HONO}]}{dt} + J_{\text{HONO}} [\text{HONO}] + k_{10}[\text{OH}][\text{HONO}] - k_3[\text{OH}][\text{NO}] \quad (\text{Eq. 12})$$

500 A quite low additional source of $(8 \pm 4) \times 10^{-9} \text{ ppbv h}^{-1}$ was derived beside OH reaction with NO.

4.3.2 Evidence for nighttime deposited HONO as a morning source

As observed in our field measurement and shown in Figure 2, the HONO always presented a strong increase from 4:00 – 7:00 (UTC). Which induces two hypotheses: (1) photolysis of
505 gas-phase and particulate nitrate, (2) dew on ground surfaces served as HONO sink during the night and become a morning source by releasing the trapped nitrite back into ambient air.

To identify this HONO source, the chemical box model as expressed in equation 10 with additional processes was extended. Heterogeneous reaction of NO_2 on the wet surface (reaction 2 in Table S1) and HONO deposition on the ground surface were firstly used to
510 quantify the contributions of the well-known HONO production and loss processes. In addition, the HONO deposition on the ground surface independent on RH (24 hours, named Model 2) and its dependence on RH (nighttime 17:00-8:00, named Model 3) were also discussed.

$$\frac{d[\text{HONO}]}{dt} = k_3[\text{OH}][\text{NO}] + k_{\text{het}} \times [\text{NO}_2] - J_{\text{HONO}}[\text{HONO}] - k_{10}[\text{HONO}][\text{OH}] - \frac{1}{4}\gamma_{\text{HONO,ground}} \times$$

515 $[\text{HONO}] \times \frac{v_{\text{HONO,ground}}}{H}$ (Eq. 13)

Both the surface production of HONO through NO_2 heterogeneous reaction and subsequent loss by ground surface deposition were already termed in equation 5 and 8, respectively. Here, $k_{\text{het}} = 0.027 \text{ h}^{-1}$ and $\gamma_{\text{HONO,ground}} = 12.5$ were applied to the model calculation to simulate the diurnal cycle of HONO. As shown in Figure 8, both Model 2 (blue line) and Model 3 (green square) cannot explain the HONO morning peak but Model 3 (green square) can well
520 reproduce the nighttime HONO, indicating that surface loss of HONO is an important sink to consider when the RH was saturated. Hence, Model 3 would be used as the basic run for the following model calculation.

To investigate the contribution of photolysis of nitric acid and nitrate ($\text{HNO}_3/\text{NO}_3^-$)
525 (reaction 8) on the diurnal HONO based on the first hypothesis, the following model calculation (Model 4) was preceded:



$$\frac{d[\text{HONO}]}{dt} = k_3[\text{OH}][\text{NO}] + k_{\text{het}} \times [\text{NO}_2] + J_{\text{HNO}_3}[\text{HNO}_3/\text{NO}_3^-] - J_{\text{HONO}}[\text{HONO}] - k_{10}[\text{HONO}][\text{OH}] - \frac{1}{4}\gamma_{\text{HONO,ground}} \times [\text{HONO}] \times \frac{v_{\text{HONO,ground}}}{H} \quad (\text{Eq. 14})$$

Where the gas-phase HNO_3 and particle NO_3^- were summed together and the photolysis frequency J_{HNO_3} was derived from the TUV model. As a result, the photolysis of $\text{HNO}_3/\text{NO}_3^-$ (Model 4, pink line) could not reproduce the HONO morning peak shown in Figure 8. This favors the second hypothesis that dew evaporation processes release HONO resulting in the sudden morning peak.

Indeed, as shown in Figure S7, the HONO morning peak always happens according to a fast decrease of RH between 4:30-9:00 (UTC). However, there is one case happened at 1:00 (UTC) on 25 April 2018, possibly due to an upcoming strong wind which decreased the RH and evaporated the dew water on the ground surface. It should be noted that this HONO morning peak was never observed during this field measurement period without a fast RH decrease, in case of rain or dry ground surface as it was observed during the morning of 23 April 2018. To figure out the relationship between temporary HONO emission from dew water and decreasing RH, the following equation was defined:

$$k_{\text{emission}} = \frac{d(\frac{\text{HONO}_{\text{unknown}}}{99.5-\text{RH}})}{dt} \quad (\text{Eq. 15})$$

where $\text{HONO}_{\text{unknown}} = \text{HONO}_{\text{measure}} - \text{HONO}_{\text{Model4}}$ was calculated for each day in the whole campaign period. Then k_{emission} could be obtained from the linear least square analysis of $\frac{\text{HONO}_{\text{unknown}}}{99.5-\text{RH}}$ vs. the internal time of HONO morning peak (4:30-7:00, UTC) as shown in Figure S8. Then the maximum and minimum of k_{emission} were obtained as 0.026 ± 0.008 and 0.006 ± 0.001 pptv $\%^{-1} \text{ s}^{-1}$, respectively, with an average of 0.016 ± 0.014 pptv $\%^{-1} \text{ s}^{-1}$ as presented in Table 4. This value was used in the following model calculation to reproduce the diurnal cycle of HONO.

$$\frac{d[\text{HONO}]}{dt} = k_3[\text{OH}][\text{NO}] + k_{\text{het}} \times [\text{NO}_2] + J_{\text{HNO}_3}[\text{HNO}_3/\text{NO}_3^-] + k_{\text{emission}} \times (99.5-\text{RH}) - J_{\text{HONO}}[\text{HONO}] - k_{10}[\text{HONO}][\text{OH}] - \frac{1}{4}\gamma_{\text{HONO,ground}} \times [\text{HONO}] \times \frac{v_{\text{HONO,ground}}}{H} \quad (\text{Eq. 16})$$

The Model 5 (red line) result in Figure 8 shows that HONO deposited to the ground surface at night was at least 90% and likely in excess of 100% of the calculated unknown HONO morning peak, which may continually serve as HONO source for the whole daytime depending on the weather condition, for example at cloudy days. These model calculations estimate that $\sim 855 \pm 427$ pptv of HONO could be released to the atmosphere from the dew evaporation during the period of 4:30-7:00 (UTC). This value is in good agreement with the HONO deposition on the ground surface of 966 ± 732 pptv presented in section 4.2.3.



560 4.3.3 HONO gradient from dew water evaporation in the morning

The morning HONO gradient (pptv) due to the dew water evaporation could be estimated from the following equation:

$$[\text{HONO}] = \frac{2 \times \text{LAI} \times F_{\text{NO}_2}}{\text{mixing height}} \quad (\text{Eq. 17})$$

F_{NO_2} is the NO_2 concentration per m^2 of the glass sampler surface. During the HONO peak at
565 6 or 7 UTC, the mixing height was 175–600 m explored by meteorological data (GDAS-data) and the mixing height ranged from 20 m to 200 m at 0:00 – 5:00 UTC. Regarding the grass height during the dew measurements (~30cm) that is approximately the height in April 2018 and May 2019, we add a factor of 6 for LAI. Hence, the morning HONO gradient was shown in Figure S9 and results in 2264.1±612.3, 1132.1±306.2, 452.8±122.5, 226.4±61.2 and
570 75.5±20.4 pptv, respectively, for a mixing height of 20, 40, 100, 200 and 600 m using the mean F_{NO_2} from 11 May 2019 for the calculation. It shows that the HONO mixing ratio within 40 m mixing height is similar with the measured HONO morning peak of 1400±100 pptv (section 4.3), which was able to detect by MARGA and LOPAP as both inlets were within this layer.

575 Indeed, few field studies (He et al., 2006; Rubio et al., 2009; Rubio et al., 2012) have reported that dew water can serve as a sink and a temporary reservoir of atmospheric HONO, but also for phenol, nitrophenols and HCHO. As shown in Figure 4, the simultaneous morning peak of NH_3 and HNO_3 suggest that the dew water also serves as a sink and a temporary reservoir of atmospheric NH_3 and HNO_3 . In addition, our dew water collection and analysis
580 found that there were 39.6–173.2 and 60.4–202.7 $\mu\text{g m}^{-2}$ in the dew samples for NH_3 and HNO_3 , respectively. However, more research on these compounds is needed. Consistently, the role of dew as a nighttime reservoir and morning source for atmospheric NH_3 has been reported by Wentworth et al. (2016). These results suggest that nocturnally deposited HONO forms a ground surface reservoir, which can be released in the following morning by dew
585 evaporation. Therefore, a significant fraction of the daytime HONO source can be explained for the Melpitz observations.

4.3.4 Impact on the primary OH sources

HONO serves as an important primary source of OH during daytime in the troposphere (Kleffmann et al., 2005; Villena et al., 2011; Kanaya et al., 2007) and Seiler et al. (2012)
590 reported that the HONO is almost the only source of OH radicals in the early morning. The morning peak of HONO is mainly released from the dew evaporation and could imply a strong supply of OH radicals and hence enhances atmospheric oxidizing capacity in the atmosphere around Melpitz. Here, the net rate of OH radical from the HONO photolysis was calculated and compared with that from ozone photolysis (reaction 11–13 in Table S1), which



595 is typically proposed as the major OH radical source in the atmosphere where water vapor is not limiting.

Other OH sources, such as photolysis of oxidized VOCs, peroxides and ozonolysis of unsaturated VOCs were not considered due to the lack of measurement data for these radical precursors. The net rate of OH production from HONO photolysis (P_{HONO}) was calculated by
600 the source strength subtracting the sink terms due to reactions (3) and (10) (Table S1). The OH production rate (P_{O_3}) from O_3 photolysis can be calculated by using the method proposed by Su et al. (2008) and (Li et al., 2018).

$$P_{\text{HONO}} = J_{\text{HONO}}[\text{HONO}] - k_3[\text{NO}][\text{OH}] - k_{10}[\text{HONO}][\text{OH}] \quad (\text{Eq. 17})$$

$$P_{\text{O}_3} = 2J(\text{O}^1\text{D})[\text{O}_3] \left(\frac{k_{12}[\text{H}_2\text{O}]}{k_{13}[\text{M}] + k_{12}[\text{H}_2\text{O}]} \right) \quad (\text{Eq. 18})$$

605 Where $J(\text{O}^1\text{D})$ was obtained from the TUV model, the temperature dependence of k_{12} and k_{13} were taken from JPL/NASA Evaluation Number 18 (Burkholder et al., 2015). As shown in Figure 9, the photolysis of HONO produced similar amounts of OH compared with photolysis of ozone at the mean daytime (9:00-14:00, UTC), as $(7.2 \pm 2.0) \times 10^5$ molecule $\text{cm}^{-3} \text{s}^{-1}$. P_{O_3} was, as expected, highest during the highest J values and negligible at the sunrise and sunset.
610 P_{HONO} had a similar trend after the noontime but presented a strong OH production around 7:00 (UTC) due to the HONO morning peak from the dew water evaporation process. These results demonstrate the significant role of HONO in the atmospheric oxidizing capacity, especially for areas that are rich of ground surface (forest and grass). In addition, the OH concentration calculated from the global radiation flux measurement was also shown in
615 yellow color of Figure 9. The different trend of calculated OH concentration compared with P_{HONO} indicate that the morning OH concentration could be highly underestimated.

5 Conclusion and Atmospheric Implications

The inter-comparison of MARGA and LOPAP for the HONO measurement was applied from 19 to 29 April 2018 at the Melpitz site. Higher HONO concentrations (~58%) were obtained
620 from MARGA compared with that of LOPAP caused by heterogeneous reactions within the MARGA WRD or potential sampling inlet artefact. However, the diurnal cycles of HONO concentrations were captured by both instruments.

The dew water NO_2^- concentration per m^2 of glass sampler surface was determined to be 7.83–9.43 $\mu\text{g m}^{-2}$. Thus, HONO gradient from dew water evaporation could be calculated and
625 ranged from 1234.1±161.9 to 41.1±5.4 pptv for mixing height of 20 to 600 m, respectively.

Well-defined diurnal cycles of HONO with concentration peaks in the early morning and in the evening were found. High time resolution of HONO measurements revealed (i) the vehicle emission is a negligible HONO source at the Melpitz site; (ii) HONO formed from the heterogeneous reaction NO_2 on the ground surface is the dominant nighttime source with a



630 high NO₂-HONO conversion frequency of 0.027±0.017 h⁻¹; (iii) significant amounts of
HONO (966±732 pptv) deposited to the ground surface at night. The accurate observations of
HONO and NO₂ allowed direct evaluation of the ground uptake coefficients for these species
at night: $\gamma_{\text{NO}_2 \rightarrow \text{HONO}_g} = 2.2 \pm 1.4 \times 10^{-5}$, $\gamma_{\text{HONO,ground}} = 12.2 \pm 4.6$. The ground uptake coefficient
635 coefficient of HONO is several magnitude higher than other study (VandenBoer et al., 2013),
which requires further exploration from controlled lab studies.

A chemical model utilizing observational constraints on the HONO chemical system based on
known sources and sinks support the hypothesis that dew water on the ground surface,
especially on leaf surfaces, behave as a sink at night and a temporary reservoir for
640 atmospheric HONO in the morning. The dew evaporation had a negative relationship with the
RH in the atmosphere and, hence, the HONO emission rate was estimated to be
0.016±0.014 pptv %⁻¹ s⁻¹ dependent on the RH after sunrise (start from 4:00, UTC, during this
campaign period). Furthermore, the formation and evaporation of dew on the ground surface
influence significantly the air-surface exchange of HONO and, thus, its temporal distributions
645 in the atmospheric boundary layer in the morning and night. The OH production rate from the
photolysis of HONO compared with that from photolysis of O₃ showed that this dew emission
of HONO can strongly enhance the OH reactivity throughout morning time and, hence, plays
a vital role in the atmospheric oxidation. Furthermore, the observed NH₃ and HNO₃ had a
similar morning behavior suggesting that some amounts of NH₃ and HNO₃ deposited in dew
650 overnight are emitted during evaporation shortly after sunrise as well. Once the dew water has
completely evaporated, their atmospheric mixing ratios either plateau or decrease.

Author contributions

RY wrote the paper. BS and GS analyzed the MARGA and dew data and wrote the paper. RY
655 and BG conducted the HONO measurement using LOPAP. TT and AW were responsible for
the particle measurement. AM and HH designed the experiments. All co-authors commented
on the manuscript.

Competing interests

660 The authors declare to have no competing interests.

Acknowledgements

The authors acknowledge financial support of this study and deployment of the MARGA
system by the German Federal Environment Agency (UBA) research foundation under
665 contracts No:351 01 093 and 351 01 070, as well as the European Union (EU) for the
Transnational access (TNA) under ACTRIS-2: Comparison of HONO-measurements with



MARGA and LOPAP at TROPOS research-site Melpitz (MARLO) is part of the project that has received funding from the European Union's Horizon 2020 research and innovation programme under grant agreement No 654109. For the laboratory analysis and the preparation
670 of solutions, we thank A. Dietze, A. Rödger and S. Fuchs. For the support especially in the field, we thank R. Rabe and A. Grüner. We thank also the TROPOS mechanical workshop for the construction of the dew sampler. The CNRS team (Orléans-France) acknowledges the support from Labex Voltaire (ANR-10-LABX-100-01) and ARD PIVOTS program (supported by the Centre-Val de Loire regional council). Europe invests in Centre-Val de
675 Loire with the European Regional Development Fund.



References

- Acker, K., Spindler, G., and Brüggemann, E.: Nitrous and nitric acid measurements during the INTERCOMP2000 campaign in Melpitz, *Atmos. Environ.*, **38**, 6497-6505, 10.1016/j.atmosenv.2004.08.030, 2004.
- 680 Aliche, B., Platt, U., and Stutz, J.: Impact of nitrous acid photolysis on the total hydroxyl radical budget during the Limitation of Oxidant Production/Pianura Padana Produzione di Ozono study in Milan, *J. Geophys. Res. Atmos.*, **107**, LOP 9-1-LOP 9-17, doi:10.1029/2000JD000075, 2002.
- Aliche, B., Geyer, A., Hofzumahaus, A., Holland, F., Konrad, S., Pätz, H. W., Schäfer, J., Stutz, J., Volz-Thomas, A., and Platt, U.: OH formation by HONO photolysis during the BERLIOZ experiment, *J. Geophys. Res. Atmos.*, **108**, PHO 3-1-PHO 3-17, doi:10.1029/2001JD000579, 2003.
- 685 Altstädter, B., Platis, A., Jähn, M., Baars, H., Lücknerath, J., Held, A., Lampert, A., Bange, J., Hermann, M., and Wehner, B.: Airborne observations of newly formed boundary layer aerosol particles under cloudy conditions, *Atmos. Chem. Phys.*, **18**, 8249-8264, 10.5194/acp-18-8249-2018, 2018.
- Ammann, M., Kalberer, M., Jost, D. T., Tobler, L., Rössler, E., Pignatelli, D., Gäggele, H. W., and Baltensperger, U.: Heterogeneous production of nitrous acid on soot in polluted air masses, *Nature*, **395**, 157, 10.1038/25965, 1998.
- 690 Ammann, M., Rössler, E., Strekowski, R., and George, C.: Nitrogen dioxide multiphase chemistry: Uptake kinetics on aqueous solutions containing phenolic compounds, *Phys. Chem. Chem. Phys.*, **7**, 2513-2518, 10.1039/B501808K, 2005.
- 695 AndresHernandez, M. D., Notholt, J., Hjorth, J., and Schrems, O.: A DOAS study on the origin of nitrous acid at urban and non-urban sites, *Atmos. Environ.*, **30**, 175-180, 10.1016/1352-2310(95)00330-2, 1996.
- Atkinson, R., Baulch, D. L., Cox, R. A., Crowley, J. N., Hampson, R. F., Hynes, R. G., Jenkin, M. E., Rossi, M. J., and Troe, J.: IUPAC Task Group on Atmospheric Chemical Kinetic Data Evaluation, *Atmos. Chem. Phys.*, **4**, 1461-1738, 2004.
- 700 Bernard, F., Cazaunau, M., Grosselin, B., Zhou, B., Zheng, J., Liang, P., Zhang, Y. J., Ye, X. N., Daele, V., Mu, Y. J., Zhang, R. Y., Chen, J. M., and Mellouki, A.: Measurements of nitrous acid (HONO) in urban area of Shanghai, China, *Environmental Science and Pollution Research*, **23**, 5818-5829, 10.1007/s11356-015-5797-4, 2016.
- 705 Birmili, W., Stratmann, F., and Wiedensohler, A.: Design of a DMA-based size spectrometer for a large particle size range and stable operation, *J Aerosol Sci*, **30**, 549-553, 10.1016/S0021-8502(98)00047-0, 1999.
- Febo, A., Perrino, C., and Cortiello, M.: A denuder technique for the measurement of nitrous acid in urban atmospheres, *Atmos. Environ.*, **27**, 1721-1728, 10.1016/0960-1686(93)90235-q, 1993.
- 710 Finlayson-Pitts, B. J., Wingen, L. M., Sumner, A. L., Syomin, D., and Ramazan, K. A.: The heterogeneous hydrolysis of NO₂ in laboratory systems and in outdoor and indoor atmospheres: An integrated mechanism, *Phys. Chem. Chem. Phys.*, **5**, 223-242, 10.1039/B208564J, 2003.
- Finlayson-Pitts, B. J.: Reactions at surfaces in the atmosphere: integration of experiments and theory as necessary (but not necessarily sufficient) for predicting the physical chemistry of aerosols, *Phys.*



- 715 Chem. Chem. Phys., 11, 7760-7779, 10.1039/b906540g, 2009.
- Genfa, Z., Slanina, S., Boring, C. B., Jongejan, P. A. C., and Dasgupta, P. K.: Continuous wet denuder measurements of atmospheric nitric and nitrous acids during the 1999 Atlanta Supersite, Atmos. Environ., 37, 1351-1364, 10.1016/S1352-2310(02)01011-7, 2003.
- 720 Größ, J., Hamed, A., Sonntag, A., Spindler, G., Manninen, H. E., Nieminen, T., Kulmala, M., Hörrak, U., Plass-Dülmer, C., Wiedensohler, A., and Birmili, W.: Atmospheric new particle formation at the research station Melpitz, Germany: connection with gaseous precursors and meteorological parameters, Atmos. Chem. Phys., 18, 1835-1861, 10.5194/acp-18-1835-2018, 2018.
- Gustafsson, R. J., Kyriakou, G., and Lambert, R. M.: The molecular mechanism of tropospheric nitrous acid production on mineral dust surfaces, ChemPhysChem, 9, 1390-1393, 10.1002/cphc.200800259, 2008.
- 725 Gutzwiller, L., Arens, F., Baltensperger, U., Gäggeler, H. W., and Ammann, M.: Significance of Semivolatile Diesel Exhaust Organics for Secondary HONO Formation, Environ. Sci. Technol., 36, 677-682, 10.1021/es015673b, 2002.
- He, Y., Zhou, X., Hou, J., Gao, H., and Bertman, S. B.: Importance of dew in controlling the air-surface exchange of HONO in rural forested environments, Geophys. Res. Lett., 33, doi:10.1029/2005GL024348, 2006.
- 730 Heland, J., Kleffmann, J., Kurtenbach, R., and Wiesen, P.: A New Instrument To Measure Gaseous Nitrous Acid (HONO) in the Atmosphere, Environ. Sci. Technol., 35, 3207-3212, 10.1021/es000303t, 2001.
- 735 Huang, G., Zhou, X. L., Deng, G. H., Qiao, H. C., and Civerolo, K.: Measurements of atmospheric nitrous acid and nitric acid, Atmos. Environ., 36, 2225-2235, 10.1016/s1352-2310(02)00170-x, 2002.
- Huang, R. J., Yang, L., Cao, J. J., Wang, Q. Y., Tie, X. X., Ho, K. F., Shen, Z. X., Zhang, R. J., Li, G. H., Zhu, C. S., Zhang, N. N., Dai, W. T., Zhou, J. M., Liu, S. X., Chen, Y., Chen, J., and O'Dowd, C. D.: Concentration and sources of atmospheric nitrous acid (HONO) at an urban site in Western China, Sci. Total Environ., 593, 165-172, 10.1016/j.scitotenv.2017.02.166, 2017.
- 740 Kalberer, M., Ammann, M., Arens, F., Gäggeler, H. W., and Baltensperger, U.: Heterogeneous formation of nitrous acid (HONO) on soot aerosol particles, J. Geophys. Res. Atmos., 104, 13825-13832, doi:10.1029/1999JD900141, 1999.
- Kanaya, Y., Cao, R., Akimoto, H., Fukuda, M., Komazaki, Y., Yokouchi, Y., Koike, M., Tanimoto, H., Takegawa, N., and Kondo, Y.: Urban photochemistry in central Tokyo: 1. Observed and modeled OH and HO₂ radical concentrations during the winter and summer of 2004, J. Geophys. Res. Atmos., 112, doi:10.1029/2007JD008670, 2007.
- 745 Kanda, Y., and Taira, M.: Chemiluminescent method for continuous monitoring of nitrous acid in ambient air, Anal. Chem., 62, 2084-2087, 10.1021/ac00218a007, 1990.
- 750 Kleffmann, J., Becker, K. H., and Wiesen, P.: Heterogeneous NO₂ conversion processes on acid surfaces: Possible atmospheric implications, Atmos. Environ., 32, 2721-2729, 10.1016/s1352-2310(98)00065-x, 1998.
- Kleffmann, J., Gavriloaiei, T., Hofzumahaus, A., Holland, F., Koppmann, R., Rupp, L., Schlosser, E., Siese, M., and Wahner, A.: Daytime formation of nitrous acid: A major source of OH radicals in a forest,



- 755 Geophys. Res. Lett., 32, doi:10.1029/2005GL022524, 2005.
- Kleffmann, J., Lörzer, J. C., Wiesen, P., Kern, C., Trick, S., Volkamer, R., Rodenas, M., and Wirtz, K.: Intercomparison of the DOAS and LOPAP techniques for the detection of nitrous acid (HONO), *Atmos. Environ.*, 40, 3640-3652, <https://doi.org/10.1016/j.atmosenv.2006.03.027>, 2006.
- Kleffmann, J., and Wiesen, P.: Technical Note: Quantification of interferences of wet chemical HONO LOPAP measurements under simulated polar conditions, *Atmos. Chem. Phys.*, 8, 6813-6822, 10.5194/acp-8-6813-2008, 2008.
- Kurtenbach, R., Becker, K. H., Gomes, J. A. G., Kleffmann, J., Lorzer, J. C., Spittler, M., Wiesen, P., Ackermann, R., Geyer, A., and Platt, U.: Investigations of emissions and heterogeneous formation of HONO in a road traffic tunnel, *Atmos. Environ.*, 35, 3385-3394, 10.1016/s1352-2310(01)00138-8, 2001.
- 765 Lahoutifard, N., Ammann, M., Gutzwiller, L., Ervens, B., and George, C.: The impact of multiphase reactions of NO₂ with aromatics: a modelling approach, *Atmos. Chem. Phys.*, 2, 215-226, 10.5194/acp-2-215-2002, 2002.
- Li, D., Xue, L., Wen, L., Wang, X., Chen, T., Mellouki, A., Chen, J., and Wang, W.: Characteristics and sources of nitrous acid in an urban atmosphere of northern China: Results from 1-yr continuous observations, *Atmos. Environ.*, 182, 296-306, <https://doi.org/10.1016/j.atmosenv.2018.03.033>, 2018.
- 770 Li, G., Lei, W., Zavala, M., Volkamer, R., Dusanter, S., Stevens, P., and Molina, L. T.: Impacts of HONO sources on the photochemistry in Mexico City during the MCMA-2006/MILAGO Campaign, *Atmos. Chem. Phys.*, 10, 6551-6567, 10.5194/acp-10-6551-2010, 2010.
- 775 Li, X., Brauers, T., Häseler, R., Bohn, B., Fuchs, H., Hofzumahaus, A., Holland, F., Lou, S., Lu, K. D., Rohrer, F., Hu, M., Zeng, L. M., Zhang, Y. H., Garland, R. M., Su, H., Nowak, A., Wiedensohler, A., Takegawa, N., Shao, M., and Wahner, A.: Exploring the atmospheric chemistry of nitrous acid (HONO) at a rural site in Southern China, *Atmos. Chem. Phys.*, 12, 1497-1513, 10.5194/acp-12-1497-2012, 2012.
- 780 Michoud, V., Kukui, A., Camredon, M., Colomb, A., Borbon, A., Miet, K., Aumont, B., Beekmann, M., Durand-Jolibois, R., Perrier, S., Zapf, P., Siour, G., Ait-Helal, W., Locoge, N., Sauvage, S., Afif, C., Gros, V., Furger, M., Ancellet, G., and Doussin, J. F.: Radical budget analysis in a suburban European site during the MEGAPOLI summer field campaign, *Atmos. Chem. Phys.*, 12, 11951-11974, 10.5194/acp-12-11951-2012, 2012.
- 785 Monge, M. E., D'Anna, B., Mazri, L., Giroir-Fendler, A., Ammann, M., Donaldson, D. J., and George, C.: Light changes the atmospheric reactivity of soot, *Proceedings of the National Academy of Sciences*, 107, 6605-6609, 10.1073/pnas.0908341107, 2010.
- Ndour, M., D'Anna, B., George, C., Ka, O., Balkanski, Y., Kleffmann, J., Stemmler, K., and Ammann, M.: Photoenhanced uptake of NO₂ on mineral dust: Laboratory experiments and model simulations, *Geophys. Res. Lett.*, 35, doi:10.1029/2007GL032006, 2008.
- 790 Pagsberg, P., Bjergbakke, E., Ratajczak, E., and Sillesen, A.: Kinetics of the gas phase reaction OH + NO(+M) → HONO(+M) and the determination of the UV absorption cross sections of HONO, *Chem. Phys. Lett.*, 272, 383-390, [https://doi.org/10.1016/S0009-2614\(97\)00576-9](https://doi.org/10.1016/S0009-2614(97)00576-9), 1997.
- Pfeifer, S., Birmili, W., Schladitz, A., Müller, T., Nowak, A., and Wiedensohler, A.: A fast and easy-to-implement inversion algorithm for mobility particle size spectrometers considering particle number size distribution information outside of the detection range, *Atmos. Meas. Tech.*, 7, 95-105,
- 795



- 10.5194/amt-7-95-2014, 2014.
- Platt, U., Perner, D., Harris, G. W., Winer, A. M., and Pitts, J. N.: Observations of nitrous acid in an urban atmosphere by differential optical absorption, *Nature*, 285, 312-314, 10.1038/285312a0, 1980.
- Rubio, M. A., Lissi, E., Villena, G., Elshorbany, Y. F., Kleffmann, J., Kurtenbach, R., and Wiesen, P.: Simultaneous measurements of formaldehyde and nitrous acid in dew and gas phase in the atmosphere of Santiago, Chile, *Atmos. Environ.*, 43, 6106-6109, 10.1016/j.atmosenv.2009.09.017, 2009.
- Rubio, M. A., Lissi, E., Herrera, N., Perez, V., and Fuentes, N.: Phenol and nitrophenols in the air and dew waters of Santiago de Chile, *Chemosphere*, 86, 1035-1039, 10.1016/j.chemosphere.2011.11.046, 2012.
- Sörgel, M., Regelin, E., Bozem, H., Diesch, J. M., Drewnick, F., Fischer, H., Harder, H., Held, A., Hosaynali-Beygi, Z., Martinez, M., and Zetzsch, C.: Quantification of the unknown HONO daytime source and its relation to NO₂, *Atmos. Chem. Phys.*, 11, 10433-10447, 10.5194/acp-11-10433-2011, 2011.
- Saliba, N. A., Yang, H., and Finlayson-Pitts, B. J.: Reaction of Gaseous Nitric Oxide with Nitric Acid on Silica Surfaces in the Presence of Water at Room Temperature, *J. Phys. Chem. A*, 105, 10339-10346, 10.1021/jp012330r, 2001.
- Sarwar, G., Roselle, S. J., Mathur, R., Appel, W., Dennis, R. L., and Vogel, B.: A comparison of CMAQ HONO predictions with observations from the Northeast Oxidant and Particle Study, *Atmos. Environ.*, 42, 5760-5770, <https://doi.org/10.1016/j.atmosenv.2007.12.065>, 2008.
- Schiller, C. L., Locquiao, S., Johnson, T. J., and Harris, G. W.: Atmospheric measurements of HONO by tunable diode laser absorption spectroscopy, *J. Atmos. Chem.*, 40, 275-293, 10.1023/a:1012264601306, 2001.
- Seiler, W., Becker, K. H., and Schaller, E.: *Tropospheric Chemistry: Results of the German Tropospheric Chemistry Programme*, Springer Netherlands, 2012.
- Spindler, G., Bruggemann, E., and Herrmann, H.: Nitrous Acid (HNO₂) Concentration Measurements And Estimation Of Dry Deposition Over Grassland In Eastern Germany, *WIT Transactions on Ecology and the Environment*, 36, 10.2495/EURO990442, 1999.
- Spindler, G., Hesper, J., Bruggemann, E., Dubois, R., Muller, T., and Herrmann, H.: Wet annular denuder measurements of nitrous acid: laboratory study of the artefact reaction of NO₂ with S(IV) in aqueous solution and comparison with field measurements, *Atmos. Environ.*, 37, 2643-2662, 10.1016/s1352-2310(03)00209-7, 2003.
- Spindler, G., Muller, K., Bruggemann, E., Gnauk, T., and Herrmann, H.: Long-term size-segregated characterization of PM₁₀, PM_{2.5}, and PM₁ at the IfT research station Melpitz downwind of Leipzig (Germany) using high and low-volume filter samplers, *Atmos. Environ.*, 38, 5333-5347, 10.1016/j.atmosenv.2003.12.047, 2004.
- Stemmler, K., Ammann, M., Donders, C., Kleffmann, J., and George, C.: Photosensitized reduction of nitrogen dioxide on humic acid as a source of nitrous acid, *Nature*, 440, 195, 10.1038/nature04603, 2006.
- Stieger, B., Spindler, G., Fahlbusch, B., Müller, K., Grüner, A., Poulain, L., Thöni, L., Seitler, E., Wallasch,



- M., and Herrmann, H.: Measurements of PM₁₀ ions and trace gases with the online system MARGA at the research station Melpitz in Germany – A five-year study, *J. Atmos. Chem.*, 75, 33-70, 10.1007/s10874-017-9361-0, 2018.
- 840 Su, H., Cheng, Y. F., Shao, M., Gao, D. F., Yu, Z. Y., Zeng, L. M., Slanina, J., Zhang, Y. H., and Wiedensohler, A.: Nitrous acid (HONO) and its daytime sources at a rural site during the 2004 PRIDE-PRD experiment in China, *J. Geophys. Res. Atmos.*, 113, doi:10.1029/2007JD009060, 2008.
- Su, H., Cheng, Y. F., Oswald, R., Behrendt, T., Trebs, I., Meixner, F. X., Andreae, M. O., Cheng, P., Zhang, Y., and Poschl, U.: Soil Nitrite as a Source of Atmospheric HONO and OH Radicals, *Science*, 333, 1616-1618, 10.1126/science.1207687, 2011.
- 845 Tuch, T. M., Haudek, A., Müller, T., Nowak, A., Wex, H., and Wiedensohler, A.: Design and performance of an automatic regenerating adsorption aerosol dryer for continuous operation at monitoring sites, *Atmos. Meas. Tech.*, 2, 417-422, 10.5194/amt-2-417-2009, 2009.
- VandenBoer, T. C., Brown, S. S., Murphy, J. G., Keene, W. C., Young, C. J., Pszenny, A. A. P., Kim, S., Warneke, C., de Gouw, J. A., Maben, J. R., Wagner, N. L., Riedel, T. P., Thornton, J. A., Wolfe, D. E., Dubé, W. P., Öztürk, F., Brock, C. A., Grossberg, N., Lefer, B., Lerner, B., Middlebrook, A. M., and Roberts, J. M.: Understanding the role of the ground surface in HONO vertical structure: High resolution vertical profiles during NACHTT-11, *J. Geophys. Res. Atmos.*, 118, 10,155-110,171, doi:10.1002/jgrd.50721, 2013.
- 855 Villena, G., Wiesen, P., Cantrell, C. A., Flocke, F., Fried, A., Hall, S. R., Hornbrook, R. S., Knapp, D., Kosciuch, E., Mauldin, R. L., III, McGrath, J. A., Montzka, D., Richter, D., Ullmann, K., Walega, J., Weibring, P., Weinheimer, A., Staebler, R. M., Liao, J., Huey, L. G., and Kleffmann, J.: Nitrous acid (HONO) during polar spring in Barrow, Alaska: A net source of OH radicals?, *Journal of Geophysical Research-Atmospheres*, 116, 10.1029/2011jd016643, 2011.
- 860 Wang, J., Zhang, X., Guo, J., Wang, Z., and Zhang, M.: Observation of nitrous acid (HONO) in Beijing, China: Seasonal variation, nocturnal formation and daytime budget, *Sci. Total Environ.*, 587, 350-359, 10.1016/j.scitotenv.2017.02.159, 2017.
- Wang, L. M., and Zhang, J. S.: Detection of nitrous acid by cavity ring down spectroscopy, *Environ. Sci. Technol.*, 34, 4221-4227, 10.1021/es0011055, 2000.
- 865 Wang, S., Zhou, R., Zhao, H., Wang, Z., Chen, L., and Zhou, B.: Long-term observation of atmospheric nitrous acid (HONO) and its implication to local NO₂ levels in Shanghai, China, *Atmos. Environ.*, 77, 718-724, 10.1016/j.atmosenv.2013.05.071, 2013.
- Wentworth, G. R., Murphy, J. G., Benedict, K. B., Bangs, E. J., and Collett, J. L., Jr.: The role of dew as a night-time reservoir and morning source for atmospheric ammonia, *Atmos. Chem. Phys.*, 16, 7435-7449, 10.5194/acp-16-7435-2016, 2016.
- 870 Wiedensohler, A.: An approximation of the bipolar charge distribution for particles in the submicron size range, *J. Aerosol Sci.*, 19, 387-389, [https://doi.org/10.1016/0021-8502\(88\)90278-9](https://doi.org/10.1016/0021-8502(88)90278-9), 1988.
- Wiedensohler, A., Birmili, W., Nowak, A., Sonntag, A., Weinhold, K., Merkel, M., Wehner, B., Tuch, T., Pfeifer, S., Fiebig, M., Fjåraa, A. M., Asmi, E., Sellegri, K., Depuy, R., Venzac, H., Villani, P., Laj, P., Aalto, P., Ogren, J. A., Swietlicki, E., Williams, P., Roldin, P., Quincey, P., Hüglin, C., Fierz-Schmidhauser, R., Gysel, M., Weingartner, E., Riccobono, F., Santos, S., Gröning, C., Faloon, K., Beddows, D., Harrison, R., Monahan, C., Jennings, S. G., O'Dowd, C. D., Marinoni, A., Horn, H. G., Keck, L., Jiang, J., Scheckman, J.,



- 880 McMurry, P. H., Deng, Z., Zhao, C. S., Moerman, M., Henzing, B., de Leeuw, G., Löschau, G., and Bastian, S.: Mobility particle size spectrometers: harmonization of technical standards and data structure to facilitate high quality long-term observations of atmospheric particle number size distributions, *Atmos. Meas. Tech.*, **5**, 657-685, 10.5194/amt-5-657-2012, 2012.
- Wiedensohler, A., Wiesner, A., Weinhold, K., Birmili, W., Hermann, M., Merkel, M., Müller, T., Pfeifer, S., Schmidt, A., Tuch, T., Velarde, F., Quincey, P., Seeger, S., and Nowak, A.: Mobility particle size spectrometers: Calibration procedures and measurement uncertainties, *Aerosol Sci. Technol.*, **52**, 146-164, 10.1080/02786826.2017.1387229, 2018.
- 885 Wohlfahrt, G., Sapinsky, S., Tappeiner, U., and Cernusca, A.: Estimation of plant area index of grasslands from measurements of canopy radiation profiles, *Agric. For. Meteorol.*, **109**, 1-12, [https://doi.org/10.1016/S0168-1923\(01\)00259-3](https://doi.org/10.1016/S0168-1923(01)00259-3), 2001.
- Wong, K. W., Oh, H. J., Lefer, B. L., Rappenglück, B., and Stutz, J.: Vertical profiles of nitrous acid in the nocturnal urban atmosphere of Houston, TX, *Atmos. Chem. Phys.*, **11**, 3595-3609, 10.5194/acp-11-3595-2011, 2011.
- 890 Xianliang, Z., Gu, H., Kevin, C., Utpal, R., and L., D. K.: Summertime observations of HONO, HCHO, and O₃ at the summit of Whiteface Mountain, New York, *J. Geophys. Res. Atmos.*, **112**, doi:10.1029/2006JD007256, 2007.
- Ye, C., Gao, H., Zhang, N., and Zhou, X.: Photolysis of Nitric Acid and Nitrate on Natural and Artificial Surfaces, *Environ. Sci. Technol.*, **50**, 3530-3536, 10.1021/acs.est.5b05032, 2016.
- 895 Yu, Y., Galle, B., Panday, A., Hodson, E., Prinn, R., and Wang, S.: Observations of high rates of NO₂-HONO conversion in the nocturnal atmospheric boundary layer in Kathmandu, Nepal, *Atmos. Chem. Phys.*, **9**, 6401-6415, 10.5194/acp-9-6401-2009, 2009.
- Zhang, B., and Tao, F.-M.: Direct homogeneous nucleation of NO₂, H₂O, and NH₃ for the production of ammonium nitrate particles and HONO gas, *Chem. Phys. Lett.*, **489**, 143-147, 10.1016/j.cplett.2010.02.059, 2010a.
- 900 Zhang, B., and Tao, F.-M.: Direct homogeneous nucleation of NO₂, H₂O, and NH₃ for the production of ammonium nitrate particles and HONO gas, *Chem. Phys. Lett.*, **489**, 143-147, 10.1016/j.cplett.2010.02.059, 2010b.
- 905 Zhang, L., Wang, T., Zhang, Q., Zheng, J., Xu, Z., and Lv, M.: Potential sources of nitrous acid (HONO) and their impacts on ozone: A WRF-Chem study in a polluted subtropical region, *J. Geophys. Res. Atmos.*, **121**, 3645-3662, doi:10.1002/2015JD024468, 2016.
- Zhou, X., Zhang, N., TerAvest, M., Tang, D., Hou, J., Bertman, S., Alaghmand, M., Shepson, P. B., Carroll, M. A., Griffith, S., Dusanter, S., and Stevens, P. S.: Nitric acid photolysis on forest canopy surface as a source for tropospheric nitrous acid, *Nature Geoscience*, **4**, 440-443, 10.1038/ngeo1164, 2011a.
- 910 Zhou, X., Zhang, N., TerAvest, M., Tang, D., Hou, J., Bertman, S., Alaghmand, M., Shepson, P. B., Carroll, M. A., Griffith, S., Dusanter, S., and Stevens, P. S.: Nitric acid photolysis on forest canopy surface as a source for tropospheric nitrous acid, *Nature Geoscience*, **4**, 440, 10.1038/ngeo1164, 2011b.
- Zhou, X. L., Gao, H. L., He, Y., Huang, G., Bertman, S. B., Civerolo, K., and Schwab, J.: Nitric acid photolysis on surfaces in low-NO_x environments: Significant atmospheric implications, *Geophys. Res. Lett.*, **30**, 10.1029/2003gl018620, 2003.
- 915



Table 1. Mean and mean error as 2 times the standard deviation of the measured HONO and the other pollutants in the Melpitz station during daytime (D, 04:00-18:00, UTC) and nighttime (N, 18:00-04:00, UTC).

	D	N		D	N
NO (ppbv)	1.0±0.5	0.5±0.3	HCl (ppbv)	0.02±0.03	0.01±0.01
NO _x (ppbv)	4±1	6±2	HNO ₂ (pptv)	424±112	541±179
NO ₂ (ppbv)	3±1	5±2	HNO ₃ (ppbv)	0.2±0.1	0.2±0.1
HONO (pptv)	162±96	254±114	NH ₃ (ppbv)	17±7	8±4
O ₃ (ppbv)	36±7	19±13	Cl ⁻ (μg m ⁻³)	0.03±0.04	0.01±0.01
SO ₂ (ppbv)	0.8±0.4	0.5±0.3	NO ₃ ⁻ (μg m ⁻³)	3±2	2±1
T (°C)	16±3	11±5	SO ₄ ²⁻ (μg m ⁻³)	1.4±0.5	1.3±0.6
RH (%)	67±7	85±11	Na ⁺ (μg m ⁻³)	0.02±0.03	0.01±0.01
Wind speed (m s ⁻¹)	3±2	1.2±0.7	NH ₄ ⁺ (μg m ⁻³)	1.1±0.7	0.8±0.4
HONO/NO _x (%)	0.04±0.02	0.05±0.02	K ⁺ (μg m ⁻³)	0	0.001±0.002
NO/NO _x (%)	0.3±0.1	0.1±0.1	Mg ²⁺ (μg m ⁻³)	0.03±0.01	0.02±0.04
OH (molecule cm ⁻³)	(2.8±0.7)×10 ⁶	(9.5±2.1)×10 ³	Ca ²⁺ (μg m ⁻³)	0.2±0.1	0.2±0.1
			NO ₂ ⁻ (μg m ⁻³)	0.01±0.01	0.03±0.02



Table 2. Nitrous acid concentration measured in dew water.

Date	Initial hour (UTC)	Final hour (UTC)	Volume (ml)	NO ₂ ⁻ (µg L ⁻¹)	F _{NO₂⁻} (µg m ⁻²)	pH
2019 8/5	18:00	5:25	76.60	41.87	2.10	6.40
		5:45	75.60	42.84	2.20	6.45
11/5	18:00	3:20	94.00	128.23	8.00	7.00
		4:20	80.00	120.43	6.40	6.90
		3:30	5:20	13.00	164.62	1.43
13/5	18:00	4:45	72.00	43.87	2.10	6.30
		5:20	79.00	58.81	3.10	6.40
14/5	18:00	5:00	15.00	148.90	1.50	6.80
		5:00	21.00	91.44	1.30	6.70



Table 3. The ratio HONO/NO₂ and the NO₂-HONO conversion frequency during nighttime.

Date	UTC	R ₂	HONO/NO ₂	k _{het} (h ⁻¹)
19/04/2018	17:30-19:50	0.45	0.121±0.011	0.043±0.002
21/04/2018	18:20-20:30	0.64	0.058±0.004	0.012±0.002
22/04/2018	18:10-21:20	0.79	0.164±0.006	0.029±0.002
25/04/2018	17:31-21:20	0.69	0.064±0.003	0.010±0.001
27/04/2018	18:00-23:41	0.48	0.116±0.007	0.016±0.001
28/04/2018	18:00-19:50	0.44	0.156±0.01	0.050±0.004
			0.113±0.044	0.027±0.017



Table 4. Summary of the temporary HONO emission rate from dew water, k_{emission} from 19 to 29 April 2018.

Period	k_{emission} (pptv % ⁻¹ s ⁻¹)	
	Min	Max
2018/4/21	0.0054	0.0357
2018/4/22	0.0048	0.0314
2018/4/24	0.0057	0.0192
2018/4/26	0.0067	0.0302
2018/4/27	0.0048	0.0215
2018/4/28	0.0079	0.017
Average	0.006±0.001	0.026±0.008

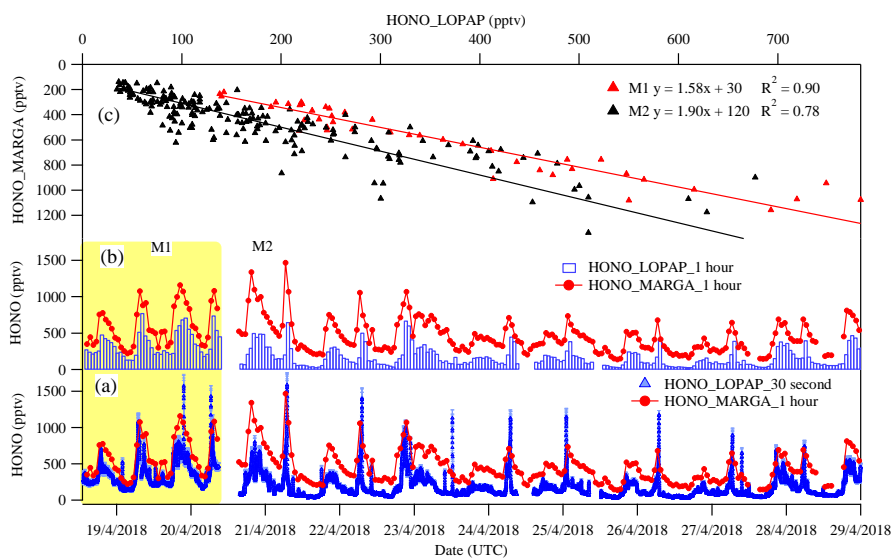


Figure 1. Time courses of HONO as hourly measured by MARGA and 30 seconds measured by LOPAP (a) and normalized hourly for LOPAP (b). (c) represents the orthogonal regression analysis between MARGA and LOPAP dependent on two different comparison period (M1 and M2).

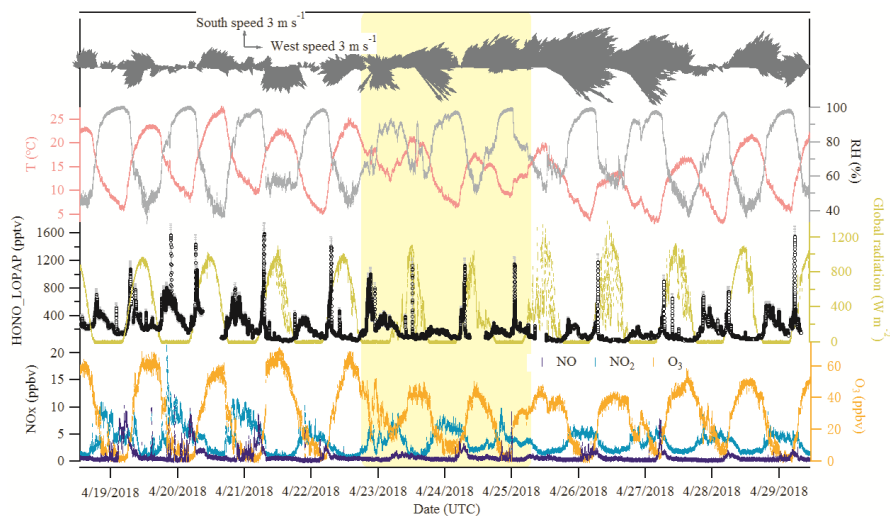


Figure 2. Time series of HONO (LOPAP measurement), NO, NO₂, O₃, global radiation, temperature (T), relative humidity (RH) and surface wind in Melpitz from 19 to 29 April 2018. The gap was mainly due to the maintenance of the instruments. The yellow shadow indicates two case events discussed in section 3.3.

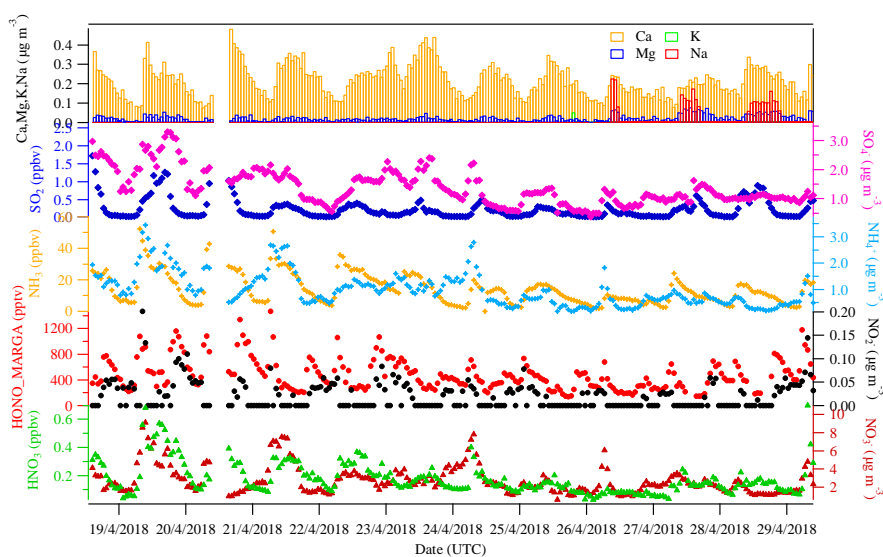


Figure 3. The hourly time-resolved quantification of water-soluble ions in PM₁₀ (NO₃⁻, SO₄²⁻, NO₂⁻, NH₄⁺, Na⁺, K⁺, Mg²⁺, Ca²⁺) and their corresponding trace gases (HONO, HNO₃, SO₂, NH₃) were measured by MARGA in Melpitz from 19 to 29 April 2018.

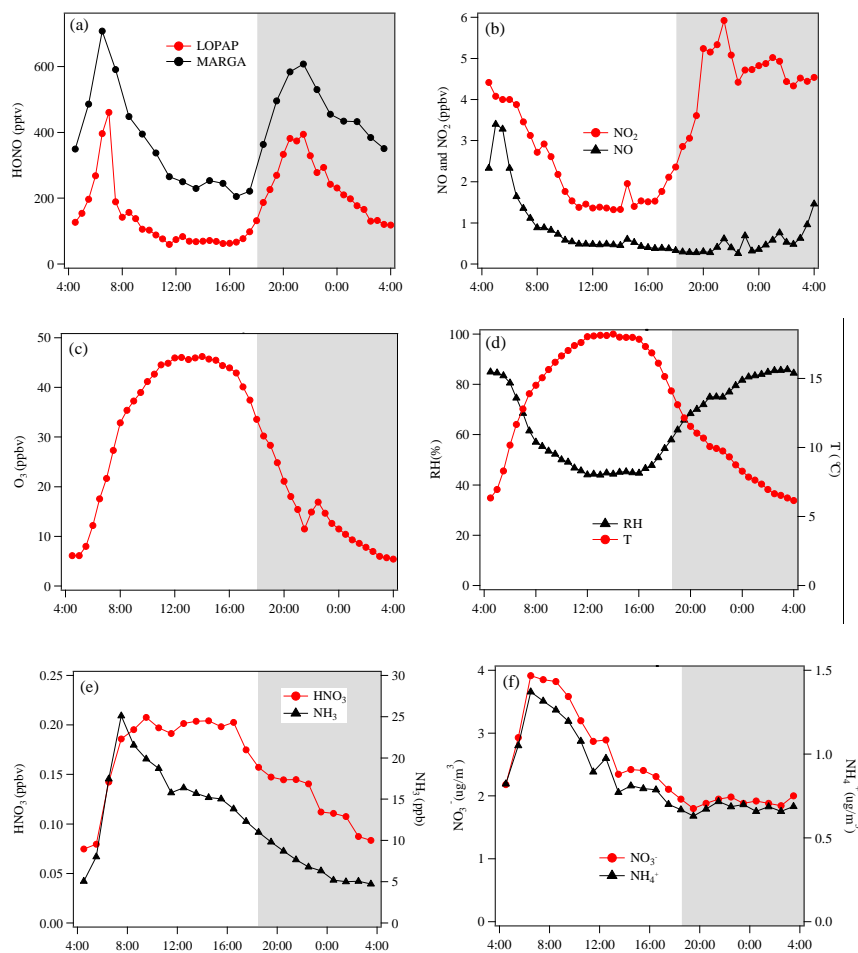


Figure 4. Diurnal variations of HONO and related species during the measurement period at Melpitz site. The grey shaded area indicates the nighttime period (18:00–04:00 UTC).

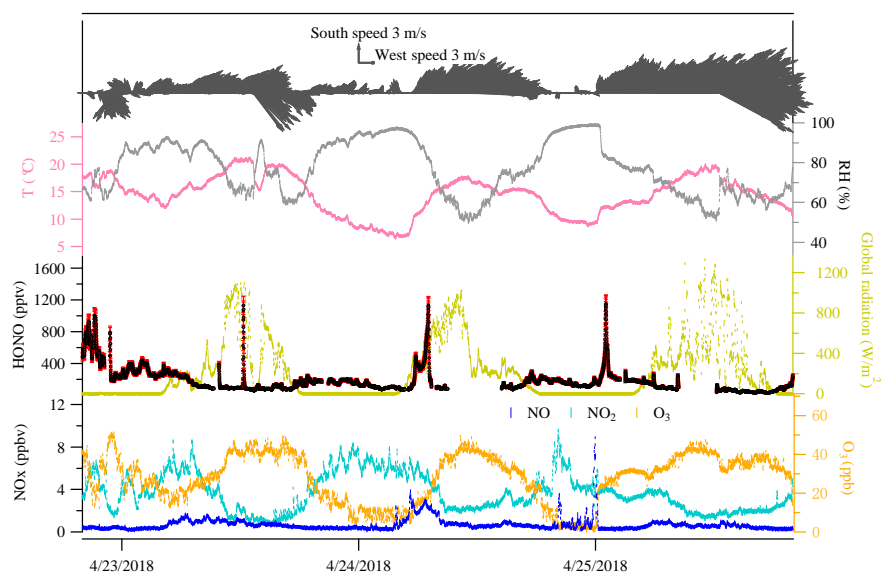


Figure 5. Case events for HONO and related species at Melpitz site during the day 23 to 25 April 2018. The red color in the HONO panel indicates the measurement error of HONO concentrations.

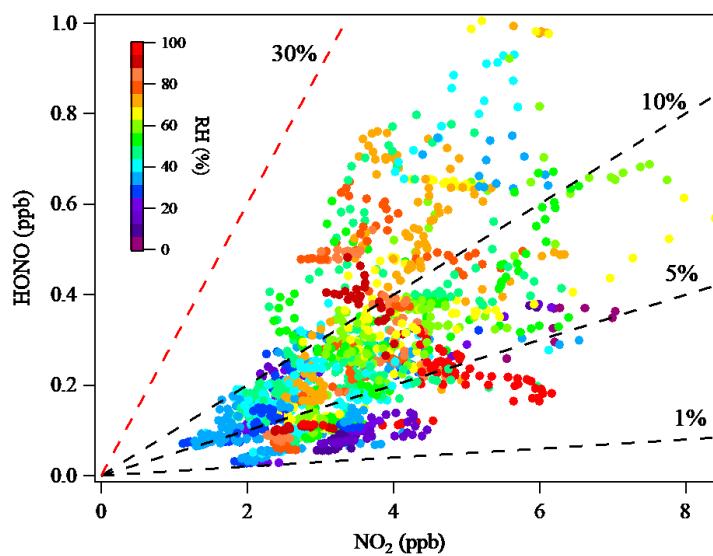


Figure 6. Correlation between HONO and NO₂ at night (17:30-00:00 UTC) during the measurement period (18-29 April 2018) at the background site of Melpitz, while the data are color coded by the relative humidity. The dashed lines correspond to the HONO/NO₂ ratio of 30% (in red), 10%, 5% and 1%.

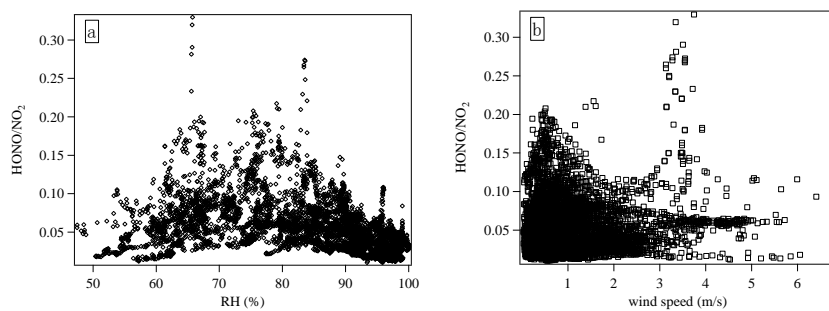


Figure 7. Scatter plot of HONO/NO₂ against RH and wind speed in the time interval of 18:00-04:00 (UTC).

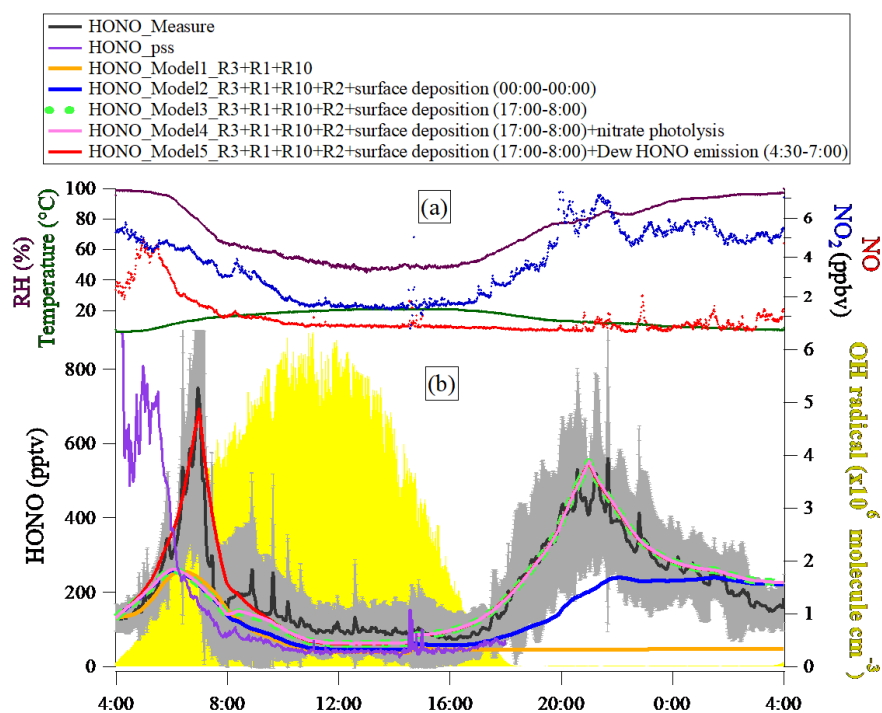


Figure 8. (a) Chemical Box model input values of measured constraints (averaged data) from 19 to 29 April 2018 for diurnal modeling of HONO chemical behavior and quantifying the missing HONO source/sink. (b) Observed average HONO atmospheric concentration (black line, $\pm 1\sigma$ in shaded area) and the model calculated HONO concentration including different HONO production and loss processes.

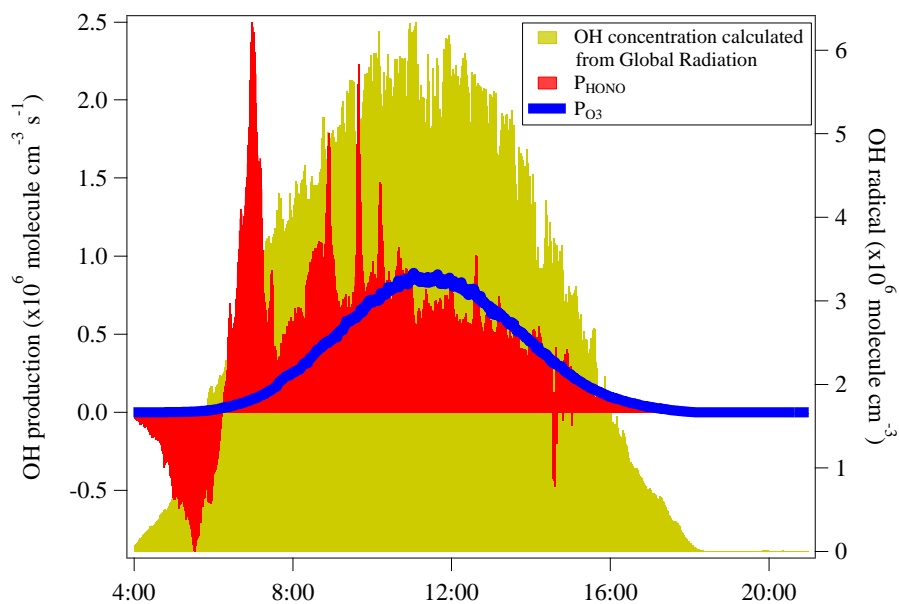


Figure 9. The OH production rates from photolysis of HONO and O₃ in Melpitz station from 19 to 29 April 2018. The OH concentration is also shown as yellow area plot, which was calculated from the global radiation flux measurement: [OH]=A*Rad taken from Größ et al. (2018).